Science of the Total Environment 916 (2024) 170133

Contents lists available at ScienceDirect

Science of the Total Environment

journal homepage: www.elsevier.com/locate/scitotenv

Characteristics of flash droughts and their association with compound meteorological extremes in China: Observations and model simulations

Yuqing Zhang [a,b,*], Qinglong You [b], Changchun Chen [c], Huaijun Wang [a], Safi Ullah [b], Liucheng Shen [d]

[a] School of Geography and Planning, Huaiyin Normal University, Huai'an 223300, China
[b] Department of Atmospheric and Oceanic Sciences & Institute of Atmospheric Sciences, Fudan University, Shanghai 200433, China
[c] School of Geographical Sciences, Nanjing University of Information Science and Technology (NUIST), Nanjing 210044, China
[d] School of Environmental and Geographical Sciences, Shanghai Normal University, Shanghai 200234, China

HIGHLIGHTS

- NEX-GDDP-CMIP6 can reasonably reflect the patterns of P − PET and flash droughts.
- The PWD falls rapidly about 1–3 pentads ahead of the soil moisture.
- Pronounced upward trends in the frequencies of flash droughts across China
- More pronounced shifts in the timing of flash droughts with higher levels of warming
- The likelihood of CMEs triggering flash droughts will increase in a warmer world.

GRAPHICAL ABSTRACT

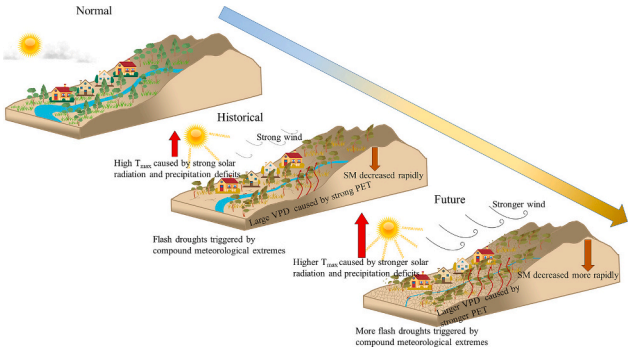

ARTICLE INFO

Editor: Anastasia Paschalidou

Keywords:
Flash droughts
Compound meteorological extremes
NEX-GDDP-CMIP6
Water deficit
China

ABSTRACT

Flash droughts have gained considerable public attention due to the imminent threats they pose to food security, ecological safety, and human health. Currently, there has been little research exploring the projected changes in flash droughts and their association with compound meteorological extremes (CMEs). In this study, we applied the pentad-mean water deficit index to investigate the characteristics of flash droughts and their association with CMEs based on observational data and downscaled model simulations. Our analysis reveals an increasing trend in flash drought frequency in China based on historical observations and model simulations. Specifically, the proportion of flash drought frequency with a one-pentad onset time showed a consistent upward trend, with the southern parts of China experiencing a high average proportion during the historical period. Furthermore, the onset dates of the first (last) flash droughts during year are projected to shift earlier (later) in a warmer world. Flash droughts become significantly more frequent in the future, with a growth rate approximately 1.3 times higher in the high emission scenario than in the medium emission scenario. The frequency of flash droughts with a one-pentad onset time also exhibits a significant upward trend, indicating that flash droughts will occur more rapidly in the future. CMEs in southern regions of China were found to be more likely to trigger flash droughts in

* Corresponding author at: School of Geography and Planning, Huaiyin Normal University, Huai'an 223300, China.
E-mail address: geonuist@foxmail.com (Y. Zhang).

https://doi.org/10.1016/j.scitotenv.2024.170133
Received 24 October 2023; Received in revised form 19 December 2023; Accepted 11 January 2024
Available online 17 January 2024

the historical period. The probability of CMEs triggering flash droughts is expected to increase with the magnitude of warming, particularly in the far-future under the high emissions scenario.

1. Introduction

The Intergovernmental Panel on Climate Change for the recent Sixth Assessment Report (IPCC AR6) highlights a global surface temperature rise of approximately 1.09 °C during the period 2011–2020 compared to 1850–1900. Notably, land areas have experienced even greater warming, with temperatures rising by 1.59 °C, compared to 0.88 °C for oceans (IPCC, 2021). This differential warming over land has significant implications for the hydrological cycle, particularly in terms of precipitation patterns. In a warmer world, precipitation variability will increase disproportionately, resulting in uneven distribution and intensification of hydroclimatic extremes (Swain et al., 2018). This can lead to the rapid onset of droughts due to short-term precipitation deficits and severe heatwaves, which ultimately have detrimental effects on crop productivity (Mohammadi et al., 2022; Svoboda et al., 2002; Xi and Yuan, 2022). In contrast to traditionally more common slow-evolving droughts, flash droughts exhibit a rapid onset accompanied by the swift depletion of water resources, causing substantial damage to ecosystems (Otkin et al., 2018; Qing et al., 2022; Wang et al., 2023b). The flash drought concept was initially proposed in the early 21st century (Svoboda et al., 2002), but gained significant attention following severe droughts in the U.S. during the summer of 2012 (Christian et al., 2021; Ford and Labosier, 2017; Mo and Lettenmaier, 2015; Mukherjee and Mishra, 2022; Otkin et al., 2016; Qing et al., 2022; Yuan et al., 2023). Flash droughts exhibit an exceptionally rapid onset, with large areas transitioning from drought-free conditions to severe drought within one month (Basara et al., 2019; Otkin et al., 2013). The swift development of these droughts poses challenges in utilizing operational forecasting models to monitor their onset, leaving limited time for stakeholders to implement appropriate measures to mitigate them and resulting in extensive crop damage and economic losses. As a result, flash drought studies have garnered considerable interest from the scientific community, ranging from regional-scale (Li et al., 2020; Nguyen et al., 2021; Zhang et al., 2021) to national-scale (Christian et al., 2019; Gong et al., 2022; Nguyen et al., 2019; Noguera et al., 2020) and global-scale (Qing et al., 2022; Sreeparvathy and Srinivas, 2022; Yuan et al., 2023) investigations. For example, Wang and Yuan (2021) indicated that anthropogenic climate change has accelerated the onset speed and intensity of droughts based on the case of a flash drought in southern China in 2019. Mishra et al. (2021) pointed out that the risk of flash droughts will increase significantly at the end of the 21st century due to a marked increase in the frequency of concurrent hot and dry extremes under anthropogenic warming scenarios.

Currently, the identification of flash droughts typically relies on indicators related to soil moisture (dryness of the land surface) (Ford and Labosier, 2017; Liu et al., 2020; Qing et al., 2022; Zhang et al., 2021), or evaporation demand (atmospheric thirst) (Basara et al., 2019; Christian et al., 2021; Nguyen et al., 2019). Soil moisture (SM) is the clearest signal for identifying flash drought events (Ford and Labosier, 2017; Osman et al., 2021), but SM observations are still relatively limited. Many scholars have identified flash droughts based on SM data from remote sensing, modeling, and reanalysis data (Liu et al., 2020; Mahto and Mishra, 2023; O and Park, 2023; Qing et al., 2022; Yuan et al., 2019; Zhang et al., 2021). However, remote sensing data generally provide SM information for shallow soil layers (0–10 cm), and the short time periods of remote sensing data can impact flash drought recognition. Additionally, individual model simulations of SM have inherent uncertainties. A multi-model ensemble mean can reduce SM fluctuations and improve flash drought identification accuracy (Zhang et al., 2021). Some researchers have approached flash drought identification from the perspective of atmospheric dryness, using indicators such as the ratio of evapotranspiration (ET) to potential evapotranspiration (PET), referred to as the evapotranspiration stress ratio (ESR) in model simulations and reanalysis data (Christian et al., 2021; Nguyen et al., 2019; Otkin et al., 2013). However, PET is often calculated using empirical equations, which introduces variability between different equations. Furthermore, the factors affecting ET are more complex than PET, leading to greater uncertainty in ESR. Recently, scholars have explored flash droughts from a simple water balance perspective, i.e., precipitation minus PET (P − PET). This approach has gained popularity due to its simplicity, fewer input variables, and ready access to high-quality data (Noguera et al., 2020; Sreeparvathy and Srinivas, 2022; Zha et al., 2023). The decline in P − PET usually precedes the intensification of a SM-based drought, making it a valuable signal for early warnings of SM-derived flash droughts (Allan, 2023; Ford and Labosier, 2017). By using P − PET to identify so-called meteorological flash droughts (Sreeparvathy and Srinivas, 2022; Zha et al., 2023), stakeholders can take appropriate measures to mitigate their damage. However, it is necessary to consider the accuracy of flash droughts in different schemes or datasets. Therefore, assessing the characteristics of flash droughts using P − PET should be based on multiple PET schemes or datasets. While SM-based flash droughts will occur at an accelerated rate in a warming climate (Qing et al., 2022; Yuan et al., 2023), it is not yet known whether this accelerated rate of onset is applicable to P − PET-derived flash droughts. In this study, we analyzed the proportions of flash droughts with a one-pentad onset time (i.e., "Case 4 events") in observations and model simulations during historical and future time periods.

Many studies have focused on flash drought characteristics during crop-growing or warm seasons, given their high occurrence probability and significant threat to crops (Gong et al., 2022; Koster et al., 2019; Liu et al., 2020; Mishra et al., 2021; Mohammadi et al., 2022; Osman et al., 2021). However, limited research has been conducted on flash drought characteristics throughout the entire year (Sreeparvathy and Srinivas, 2022), particularly regarding the onset dates of the first and last flash droughts. Investigating these onset dates is crucial, as climate warming is expected to shift the timing of heatwaves and droughts earlier or later in the year (Mo, 2011; Shi et al., 2021). Therefore, there is a clear imperative to determine the characteristics of onset dates of the annual first and last flash droughts, particularly under different future emissions scenarios. Analyzing these onset dates will yield valuable insights for a comprehensive understanding of flash drought characteristics and how to effectively predict them.

Global climate models play an important role in studying hydroclimatic extremes and their impacts (Chiang et al., 2018; Jiang et al., 2015; Su et al., 2018; Zhang et al., 2016). The Coupled Model Intercomparison Project Phase 6 (CMIP6) has improved evaluations and projections in various aspects of the climate, such as precipitation and temperature averages and extremes (Fischer et al., 2021; Meng et al., 2022; Zhu et al., 2021). CMIP6 combines the shared socioeconomic pathway (SSP) and representative concentration pathway (RCP) to provide realistic projections of future climate change (Eyring et al., 2016; O'Neill et al., 2016). For example, the SSP245 scenario (i.e., moderate emission) is a combination of SSP2 and RCP4.5 scenarios; SSP585 (high emission) is a combination of SSP5 and RCP8.5. Despite the utility of CMIP6, its application in assessing and projecting flash droughts is still very limited (Sreeparvathy and Srinivas, 2022; Yuan et al., 2023). The coarse resolutions of the original CMIP6 models prevent more fine-grained assessments or predictions of flash droughts at regional or national scales. Previous studies using SM as an indicator have shown that flash droughts can occur more rapidly under climate warming (Qing et al., 2022; Yuan et al., 2023). However, it remains unclear whether similar trends exist for P − PET-derived flash droughts.

Therefore, we investigated the projected changes in P − PET-derived flash droughts using downscaled CMIP6 model simulations under different scenarios.

Flash droughts are typically the result of a combination of factors, including heat, precipitation deficits, and strong evapotranspiration leading to a rapid depletion of SM (Mishra et al., 2021; Qing et al., 2022). These compound meteorological extremes (CMEs) can trigger the occurrence of flash droughts and exacerbate their severity. For example, extreme dry conditions caused by high temperatures and precipitation deficits in southern China in August of 2019 resulted in flash droughts (Wang and Yuan, 2021). Similarly, the likelihood of triggering a flash drought is expected to increase across India due to the projected amplification of compound hot and dry extremes in the future (Mishra et al., 2021). While previous studies have primarily focused on analyzing individual meteorological variables before, during, and after flash droughts (Ford and Labosier, 2017; Li et al., 2020; Zhang et al., 2021), the relationship between CMEs and flash droughts is not yet fully understood. Therefore, we sought to determine the likelihood of CMEs triggering flash droughts both in historical periods and under future projected climate conditions in this study.

The main objectives of this study included analyzing the characteristics of flash droughts and their relationship with CMEs in China based on observations and 24 downscaled CMIP6 outputs. The specific goals include: (1) analysis of the applicability of P − PET-derived flash droughts based on multi-source datasets; (2) assessment of flash drought characteristics in downscaled CMIP6 simulations, with special focus on the most rapidly occurring category; (3) investigation of onset dates of first and last flash droughts in a warmer world; and (4) exploration of the relationships between flash droughts and CMEs. The outcomes of this study may contribute to refinement of the definition of flash drought and enhanced knowledge of the relationship between flash droughts and CMEs. Ultimately, our findings may provide a foundation for prediction and early warning systems for flash droughts, thereby supporting proactive measures to mitigate their effects.

2. Materials and methods

2.1. Data

Daily precipitation, maximum temperature (T_{max}), minimum temperature (T_{min}), mean temperature, relative humidity (RH), and wind speed spanning the period of 1981–2020 were gathered from approximately 2400 meteorological observations of the National Meteorological Information Center of the China Meteorological Administration (http://data.cma.cn/). To ensure data continuity and integrity, stations with missing values exceeding 3 % of the total daily series within 1981–2020 were excluded. The missing values of the remaining data were estimated using the nearest neighbor interpolation method based on values for neighboring stations on the same day. Ultimately, 2301 meteorological stations across China were selected, with each station providing multiple meteorological variables for 1981–2020.

The fifth-generation reanalysis dataset (ERA5) was downloaded from the European Centre for Medium-Range Weather Forecasts (Hersbach et al., 2020), providing a comprehensive set of hydrometeorological variables with high spatiotemporal resolution. It is an enhanced version of ERA-Interim that was constructed using a 4D-Var assimilation method, which combines multiple data sources with advanced physical processes. ERA5 has been widely utilized in hydrometeorological explorations (Di Napoli et al., 2021; Jiang et al., 2021a; Martius et al., 2016; Zhang et al., 2019). For this study, hourly variables from ERA5 were aggregated and processed to derive daily information, ensuring compatibility with our analysis. To align with the timespan of the observations, we utilized the ERA5 reanalysis dataset to obtain precipitation, PET, surface net solar radiation, surface net thermal radiation, and SM data for 1981–2020. The SM data includes three layers (i.e., 0–7 cm, 7–28 cm, and 28–100 cm). We aggregated SM values of 0–28 cm and 0–100 cm layers using different soil layer thickness weighting methods.

The Global Land Evaporation Amsterdam Model version 3.5a (GLEAM3.5a), which incorporates satellite observations, reanalysis data, and ground-based observations, is a widely used resource in hydroclimatic research (Jiang et al., 2021b; Martens et al., 2017; Qing et al., 2022; Yang et al., 2017). We used the PET and SM from GLEAM 3.5a during 1981–2020 for the purposes of this study. The SM information in GLEAM3.5a was divided into two layers: the surface layer (i.e., 0–10 cm) and root-zone layer. The depth of the root-zone layer varies depending on the vegetation type, typically ranging from 10 to 100 cm for low vegetation types and from 10 to 250 cm for tall vegetation. We focused on a maximum soil depth of 100 cm, using the 10–100 cm thickness of the root-zone layer from GLEAM3.5a as our representative SM data. The 0–100 cm SM data from GLEAM3.5a was computed by combining the weights of 0–10 cm (surface) and 10–100 cm (root-zone) soil layer thicknesses. Additionally, the Chinese land surface hydrological dataset (i.e., VIC-CN05.1) provided surface (i.e., 0–10 cm) SM during 1981–2015 (Miao and Wang, 2020).

The NASA Earth Exchange Global Daily Downscaled Projections (NEX-GDDP) dataset has been widely utilized in historical assessments and future projections for climate research across global and regional scales (Lafferty et al., 2021; Raghavan et al., 2018; Zhang et al., 2019). NEX-GDDP-CMIP6 was released as the latest version in 2022 and includes downscaled outputs from 35 models based on the original CMIP6 simulations (Thrasher et al., 2022): 1950–2014 for historical and 2015–2100 for future periods. The NEX-GDDP-CMIP6 dataset was developed using the bias-correction and spatial-disaggregation (BCSD) approach to uniformly downscale the original CMIP6 simulations to a spatial resolution of 0.25° based on a global meteorological dataset of assimilated observations and reanalysis information. NEX-GDDP-CMIP6 accurately reflects the characteristics of precipitation and temperature (both averages and trends) in China (Zhang et al., 2023b). Detailed information and documentation regarding the NEX-GDDP-CMIP6 dataset are available online at https://www.nccs.nasa.gov/services/data-collections/land-based-products/nex-gddp-cmip6. To ensure consistency in variables, scenarios, and timespans, 24 downscaled model simulations (Table S1) were selected across China. The variables include daily precipitation, T_{max}, T_{min}, RH, and wind speed from three experimental categories: historical (1981–2014), SSP245 (2015–2100), and SSP585 (2015–2100).

2.2. Estimation of PET

PET is difficult to monitor with instruments and is generally calculated by empirical equations. Commonly accepted Penman-Monteith and Thornthwaite methods (Su et al., 2018; Trenberth et al., 2014; Vicente-Serrano et al., 2010; Zhang et al., 2023b) were used in this study to estimate daily PET. The Penman-Monteith equation recommended by the Food and Agriculture Organization (FAO) was used to calculate daily PET (Allen et al., 1998) as follows:

$$PET_{PM} = \frac{0.408 \bullet \Delta \bullet (R_n - G) + \gamma \bullet \frac{900}{T+273} \bullet U_2 \bullet (e_s - e_a)}{\Delta + \gamma \bullet (1 + 0.34 \bullet U_2)} \quad (1)$$

where PET_{PM} is the PET (mm•day^{-1}), Δ is the slope of the saturation vapour pressure curve (kPa•°C^{-1}), R_n is the net surface radiation (MJ•m^{-2}•day^{-1}), G is the soil heat flux (MJ•m^{-2}•day^{-1}), γ is the psychrometric constant (kPa•°C^{-1}), T is the daily mean surface air temperature (°C), U_2 is the daily mean wind speed at 2 m height (m/s), e_s is the saturation vapour pressure (kPa), and e_a is the actual vapour pressure (kPa). The variable Δ can be computed as follows:

$$\Delta = \frac{4098 \bullet \left[0.6108 \bullet exp\left(\frac{17.27 \bullet T}{T+237.3}\right)\right]}{(T+237.3)^2} \quad (2)$$

where T is calculated from the average daily T_{max} and T_{min} recommended by the FAO. R_n is the difference between incoming and outgoing radiation of both short and long wavelengths, which can be calculated using the net thermal and solar radiation at the surface in ERA5. In general, the soil heat flux (G) during a 10-day period is relatively slight and can be ignored. γ can be calculated as follows:

$$\gamma = 0.00665 \bullet P \tag{3}$$

where P is the atmospheric pressure (kPa), which can be calculated as follows:

$$P = 101.3 \bullet \left(\frac{293 - 0.0065 \bullet z}{293}\right)^{5.26} \tag{4}$$

where z is the local elevation above sea level (m). The wind speed at the Chinese weather station is defined as the wind speed at 10 m. The 2-m-height wind speed values can be calculated as follows:

$$U_2 = U_H \bullet \frac{4.87}{ln(67.8 \bullet H - 5.42)} \tag{5}$$

where U_2 is the wind speed at 2 m (m/s), H is the height of the anemometer instrument placed above the ground ($H = 10$ m), and U_H is the wind speed value at 10 m (m/s) from the meteorological station. The numerical relationship between saturation vapour pressure and air temperature is:

$$e^0(T) = 0.6108 \bullet exp\left(\frac{17.27 \bullet T}{T + 237.3}\right) \tag{6}$$

where $e^0(T)$ is the saturation vapour pressure (kPa) at an air temperature of T (°C). FAO recommends the following formula to calculate the saturation vapour pressure (e_s):

$$e_s = \frac{e^0(T_{max}) + e^0(T_{min})}{2} \tag{7}$$

where e_s is the average of the saturation vapour pressure at the daily T_{max} and T_{min}. The actual vapour pressure (e_a) can be computed as:

$$e_a = e_s \bullet \frac{RH}{100} \tag{8}$$

where RH denotes the relative humidity (0−100).

The Thornthwaite method uses temperature and latitude data to estimate PET, and is relatively simple to compute as it has few input variables (Thornthwaite, 1948). In this study, the modified Thornthwaite method (Pereira and Pruitt, 2004) was used to calculate daily PET:

$$PET_{TH} = \begin{cases} C \bullet \left(-415.85 + 32.24 \bullet T_{ef} - 0.43 \bullet T_{ef}^2\right), T_{ef} \geq 26°C \\ 16 \bullet C \bullet \left(\frac{10 \bullet T_{ef}}{I}\right)^a, 0°C < T_{ef} < 26°C \\ 0, T_{ef} \leq 0°C \end{cases} \tag{9}$$

where T_{ef} is daily effective temperature. When T_{ef} is daily average temperature, the calculated PET is denoted as TH. T_{ef} can also be derived as follows:

$$T_{ef} = 0.5 \bullet k \bullet (3 \bullet T_{max} - T_{min}) \tag{10}$$

where k is calibration coefficient, which is commonly set to 0.65, 0.69, or 0.72 (Chang et al., 2019; Pereira and Pruitt, 2004; Trajkovic et al., 2019). The PET derived from these three values are denoted as TH65, TH69, and TH72 in this study. I is the thermal index, which reflects the local normal climate temperature regime:

$$I = \sum_{n=1}^{12} (0.2 \bullet T_n)^{1.514} \tag{11}$$

where T_n is the monthly average temperature (°C; if negative, 0 is used). The exponent a is a function of I:

$$a = 6.75 \times 10^{-7} \bullet I^3 - 7.71 \times 10^{-5} \bullet I^2 + 1.7912 \times 10^{-2} \bullet I + 0.49239 \tag{12}$$

A conversion factor C is required to convert the PET from monthly scale to daily scale. $C = N/360$, where N is the photoperiod (h) for a given day, which is calculated using latitude and Julian day information as follows:

$$\delta(J) = 0.409 \bullet sin\left(\frac{2\pi}{365} \bullet J - 1.39\right) \tag{13}$$

$$\omega_s(J) = arcos[-tan(\theta) \bullet tan(\delta)] \tag{14}$$

$$N(J) = \frac{24}{\pi} \bullet \omega_s(J) \tag{15}$$

where δ is the declination angle (radians), J is the Julian day in the year, ω_s is the sunset angle (radians), θ is the latitude (radians), and N is the daily daylight hours.

2.3. Flash drought definition

The 40th percentile of drought-related variables (e.g., SM and ESR) was used as the critical threshold for dryness characteristics (Christian et al., 2021; Ford and Labosier, 2017). We processed all daily hydroclimatic variables into pentad-mean (5-day average) series. There are 73 pentads in a year (excluding February 29 in leap years). The flash drought onset was defined as a decline in pentad-mean SM or ESR from ≥40 % to ≤20 % within 4–6 pentads, which is a key criterion employed in previous studies (Christian et al., 2021; Ford and Labosier, 2017; Yuan et al., 2023; Zhang et al., 2021). Accordingly, we used the pentad-mean water deficit index (PWD=P–PET) as the base variable for identifying flash droughts. Flash droughts can occur in any season throughout the year in China, so we investigated the flash drought characteristics based on pentad-mean PWD in both historical and future periods.

We classified flash droughts into four specific cases (scenarios) for analysis (Supplementary Materials, Fig. S1).

$$\text{Case 1} = \begin{cases} \text{PWD}\left(t_{pre1}\right) \geq 40^{th}\text{ percentile} \\ 20^{th}\text{ percentile} < \text{PWD}\left(t_{1,2}\right) < 40^{th}\text{ percentile} \\ \text{PWD}\left(t_{3,\ldots,n}\right) \leq 20^{th}\text{ percentile}, 6 \leq n \leq 18 \end{cases} \tag{16}$$

$$\text{Case 2} = \begin{cases} \text{PWD}\left(t_{pre1}\right) \geq 40^{th}\text{ percentile} \\ 20^{th}\text{ percentile} < \text{PWD}\left(t_1\right) < 40^{th}\text{ percentile} \\ \text{PWD}\left(t_{2,\ldots,n}\right) \leq 20^{th}\text{ percentile}, 5 \leq n \leq 18 \end{cases} \tag{17}$$

$$\text{Case 3} = \begin{cases} \text{PWD}\left(t_{pre1}\right) \geq 40^{th}\text{ percentile} \\ \text{PWD}\left(t_1\right) \leq 20^{th}\text{ percentile} \\ 20^{th}\text{ percentile} < \text{PWD}\left(t_2\right) < 40^{th}\text{ percentile} \\ \text{PWD}\left(t_{3,\ldots,n}\right) \leq 20^{th}\text{ percentile}, 6 \leq n \leq 18 \end{cases} \tag{18}$$

$$\text{Case 4} = \begin{cases} \text{PWD}\left(t_{pre1}\right) \geq 40^{th}\text{ percentile} \\ \text{PWD}\left(t_{1,\ldots,n}\right) \leq 20^{th}\text{ percentile}, 5 \leq n \leq 18 \end{cases} \tag{19}$$

where $PWD(t_{pre1})$ indicates the PWD before one pentad of flash drought onset. The rate of intensification (RI) for PWD is denoted as the current pentad value minus the previous pentad value. The RI3 value (i.e., the average of three change values generated in t_{pre1} to t_3) of the first four-pentad PWD was utilized to monitor flash drought onset. The variables t_1 and t_n indicate the start and end dates of flash droughts, respectively.

The four cases (scenarios) in this study have the following characteristics: (1) the PWD percentile decreases from ≥40th percentile (t_{pre1}) to ≤20th percentile within a four-pentad period; (2) the RI3 is not less than the 6.6th percentile; (3) the duration of a drought (PWD ≤ 20th percentile) is at least four pentads (one pentad more than the duration of drought identified by SM, which can cause substantial impacts); (4) the minimum duration of a flash drought is five pentads and the maximum duration is 18 pentads to distinguish it from a longer-term drought. The flash drought is considered to end when PWD increases to above the 20th percentile. It is generally characterized by an increasing onset speed from Case 1 to Case 4 of flash droughts.

2.4. Compound meteorological extremes

CMEs were defined here by the simultaneous occurrence of extreme conditions in two or more variables at the same pentad and location. The extreme threshold for CMEs was set as the 90th percentile based on long-term pentad series (observations for 1981–2020 and model simulations for 1981–2014). Four types of CME were identified: compound high temperature and atmospheric drying events (T_{max} > 90th percentile and VPD > 90th percentile, termed compound T_{max} & VPD events), compound high temperature and strong winds (T_{max} > 90th percentile and Wind >90th percentile, termed compound T_{max} & Wind events), compound atmospheric drying events and strong winds (VPD > 90th percentile and Wind >90th percentile, termed compound VPD & Wind events), and compound high temperature, atmospheric drying events, and strong winds (T_{max} >90th percentile, VPD > 90th percentile, and Wind >90th percentile, termed compound T_{max} & VPD & Wind events). The presence of CMEs during a flash drought suggests the probability of CMEs inducing the flash drought. The relationship between CMEs and flash droughts is quantified here as the proportion (P_n) of the number of CMEs occurring during flash droughts to the total number of CMEs:

$$P_n = \frac{N_{CE}}{T_{CE}} \times 100\% \tag{20}$$

where P_n denotes the proportion, N_{CE} is the number (pentads) of a certain type of CME occurring during a flash drought, and T_{CE} is the total number (pentads) of such CME.

2.5. Standardized anomaly

Standardized meteorological and SM variables (e.g., PET, VPD, and SM) were utilized to reflect drought stress signals. The standardized anomaly can be calculated as follows (O and Park, 2023):

$$A_{i,j} = \frac{X_{i,j} - \overline{X_j}}{\sigma_i} \tag{21}$$

where $A_{i,j}$ denotes the X anomaly in the pentad j of year i, $\overline{X_j}$ refers to the mean X value in the pentad j during 1981–2020, and σ_i is the standard deviation of X in the pentad j from 1981 to 2020.

3. Results

3.1. Historical variations of flash droughts

The Thornthwaite method with an effective temperature parameter of 0.69 (TH69) provides PET results more comparable to those obtained by the Penman-Monteith (PM) equation (Supplementary Materials, Fig. S2). This alignment translates to a more consistent frequency of flash droughts for both types of PET methods (Supplementary Materials, Figs. S3 and S4). Therefore, we applied 24 NEX-GDDP-CMIP6 model simulations to evaluate flash droughts using TH69 PET and precipitation.

P − PET was a key variable for calculating flash droughts in this study. Accordingly, we evaluated the characteristics of historical (1981–2014) P − PET from NEX-GDDP-CMIP6 data to predict future changes in flash droughts. The spatial distributions of P − PET in the observation data (Fig. 1a) and the multi-model ensemble mean (MME) (Fig. 1b) were basically consistent, with the annual mean P − PET values decreasing from >600 mm in southeastern parts of China to < −600 mm in northwestern parts of China. This also suggests that southeastern parts of China are characterized by a distinctly humid climate, whereas northwestern parts of China are characterized by a distinctly dry climate. To assess the models' ability to simulate the temporal features of P − PET trends, we compared the model-simulated P − PET trends for the historical period with the observations. Using the 10th–90th percentile range of observational station or model grid data, we assessed how accurately the models reflect the P − PET trends. As depicted in Fig. 1c, our observations revealed more pronounced drying trends of P − PET than wetting trends (about −76 to 17 mm/decade) due to regional variations in precipitation and evapotranspiration across regions. With the exception of the EC-Earth3 model, which exhibited a clear wetting trend, the other model simulations showed trend values falling roughly within the 10th–90th percentile of the observations. The 10th–90th percentile range of MME P–PET trends was about −42 to 17 mm/decade, which was smaller than the range of observed values. Overall, the NEX-GDDP-CMIP6 models effectively reflect the spatial and long-term trend characteristics of P − PET, suggesting a high degree of reliability in characterizing future flash droughts.

We considered observed flash droughts identified via station-observed precipitation and the seven PET methods as benchmarks (observations). Flash droughts identified using each model's precipitation and TH69 PET method were considered as model simulations. The spatial patterns of the observations and MME were broadly consistent (Fig. 2a–b), with higher flash drought frequencies in the northern and southern parts of China. The MME slightly exceeded the observed values, as exemplified in Jiangxi Province where the mean frequency was 5 events/decade in the observations and 6 events/decade in the model simulations. Generally, the absolute differences in frequencies were within a range of −1 to 2 events/decade (Fig. 2c). This suggests that MME reasonably reflects the spatial frequencies of flash droughts. Regarding the proportion of Case 4 (i.e., one-pentad onset time) flash droughts, the spatial patterns of the multi-observation and multi-model ensemble means were similar (Fig. 2d–e), with the overall proportion values decreasing from >65 % in the south to <40 % in the north. This indicated a higher rapidity of flash droughts in southern China, allowing less time for effective response measures. Case 4 proportions of the MME were slightly lower than those of the multi-observation ensemble mean. The absolute differences in Case 4 proportions for MME in most regions fell within −20 % to 10 % (Fig. 2f).

The observations clearly indicated an upward trend in flash drought frequency across China, with an average trend of 0.029 events/decade (Fig. 3a). The MME also exhibited a clear increasing trend, with an average trend of 0.019 events/decade (Fig. 3b), though this increase was smaller than the observed value. The proportion of Case 4 flash droughts also showed a clear upward trend, with average increases of 1.768 %/decade (Fig. 3c) and 0.504 %/decade (Fig. 3d) for the multi-observation and multi-model ensemble means, respectively. Annual total frequency changes in flash droughts identified by the seven PET methods were relatively consistent, as were the annual proportions of Case 4 frequency. However, the MME slightly underestimated the trend values for frequencies and Case 4 proportions of flash droughts in the historical periods. Overall, a clear upward trend in flash drought frequency across China identified in both observations and simulations, accompanied by a pronounced upward trend in the proportion of Case 4 events. A severe flash drought event occurred in southern China in August 2019 with extreme speed and intensity due to a strong cyclonic anomaly over northwestern parts of the Pacific and a persistent local geopotential height anomaly (Wang and Yuan, 2021). This drought devastated millions of hectares of crops, resulting in serious economic losses (Chen et al., 2023a; Jiang et al., 2022).

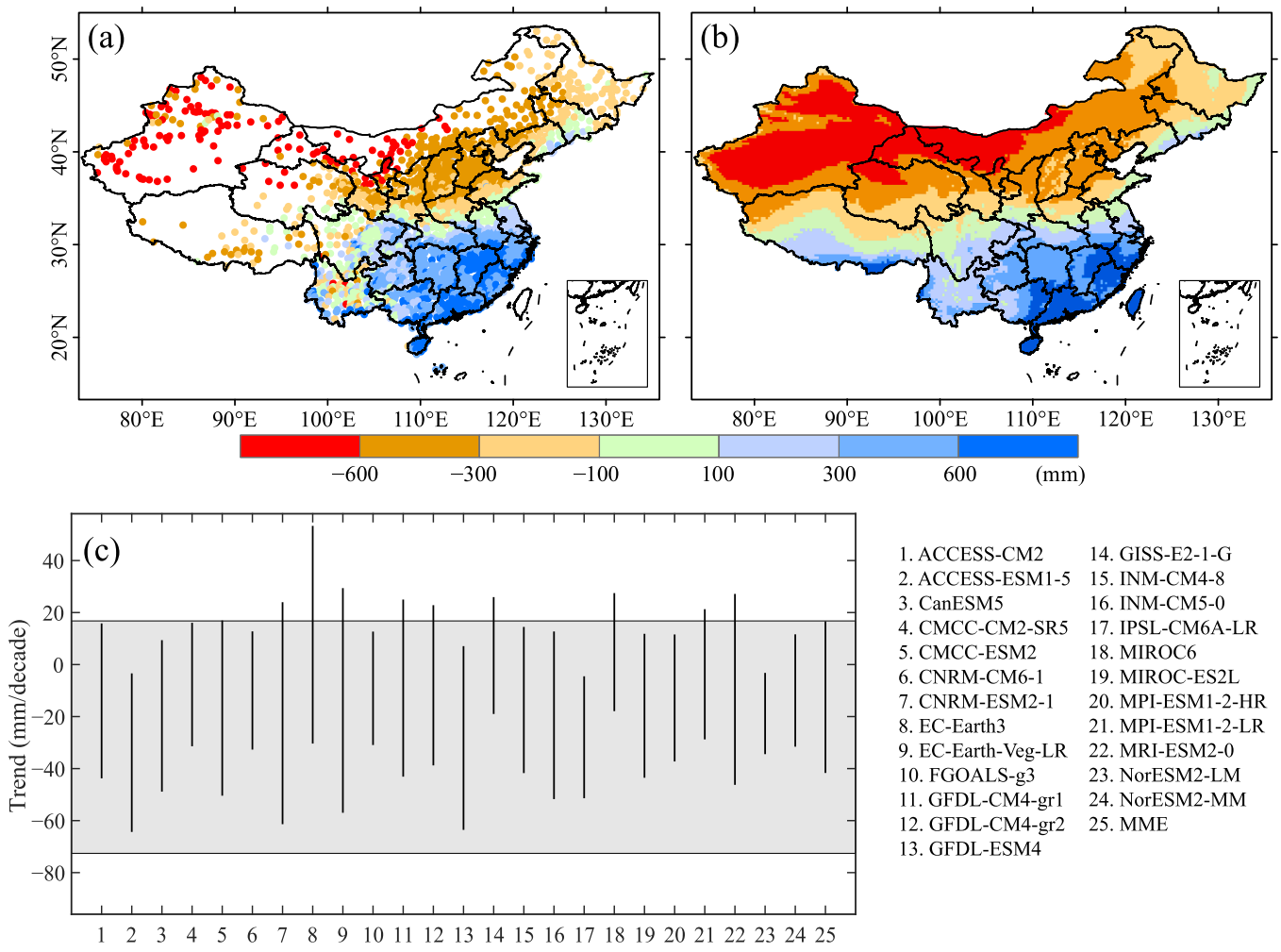

Fig. 1. Spatial patterns of annual mean P − PET in the historical period based on (a) observation (stations) and (b) 24 model-ensemble mean (MME) of NEX-GDDP-CMIP6. (c) The 10th–90th percentile range of historical P − PET trends in China is based on observations (grey band) and each model simulations (historical period: 1981–2014). PET calculations are based on the TH69 method in both observational and model data.

3.2. Flash drought onset date characteristics

We explored changes in occurrence dates of flash droughts, focusing on the onset date difference (expressed in pentads of the year) for the first (last) flash droughts. The onset date difference was calculated as the latter period of the first (last) flash drought minus the earlier period of the first (last) drought, serving as an early (delayed) signal for flash drought. As shown in Fig. 4, negative onset date differences indicate an earlier occurrence of flash droughts in the latter period compared to the earlier period. Conversely, a positive difference indicates a delayed onset. In the latter period (2001−2020) of historical observations, the first flash drought event occurred earlier at approximately 50–60 % of the stations compared to the previous period (1981–2000) across China (Fig. 4a). This suggests that in a warming world, the occurrence date of the first flash drought event will be earlier, particularly in the northeastern and Yangtze-Huai River regions (Supplementary Materials, Fig. S5). The spatial date differences of the first flash drought event in the model simulations were generally consistent with the observations (Supplementary Materials, Fig. S6). Over half of the area exhibited a negative date difference in the model simulations, indicating an earlier occurrence of the first annual flash drought event in the latter period compared to the earlier period. As shown in Fig. 4b, the last flash drought event occurred later at about 50–60 % of the stations during 2001–2020 compared to 1981–2000. This suggests that under global warming, there is an increased likelihood of a delay in the date of the last flash drought event, particularly in the northeastern and southern parts of China (Supplementary Materials, Figs. S7 and S8). The MME reasonably reflected the date difference of the first and last flash drought events in the historical period.

Under the SSP245 scenario, approximately 50–60 % of grids showed an earlier date for the first flash drought event during 2032–2065 compared to 1981–2014 (Fig. 4c), while about 60–70 % of grids showed an earlier date for the first flash drought event during 2066–2099 compared to 1981–2014. This suggests a significant increase in the number of regions experiencing an earlier first flash drought event in the mid to late 21st century. Similarly, about 55–65 % of grids exhibited a later date for the last flash drought event during 2032–2065 compared to 1981–2014 under the SSP245 scenario (Fig. 4d), while about 65–75 % of grids showed a later date for the last flash drought event during 2066–2099 compared to 1981–2014. This indicated a notable increase in the regions with a delayed last flash drought event during the mid to late 21st century. The date difference proportions were more pronounced under SSP585 than SSP245 scenarios (Fig. 4e–f). For example, under the SSP585 scenario, as much as 75–85 % of grids exhibited earlier dates for first flash drought events while 80–85 % of grids showed later dates for last flash drought events during 2066–2099 compared to 1981–2014. The spatial date differences in model simulations further support the notion that the first flash drought event of the year will occur earlier and the last flash drought event will occur later for the vast majority of China during the mid to late 21st century under high-

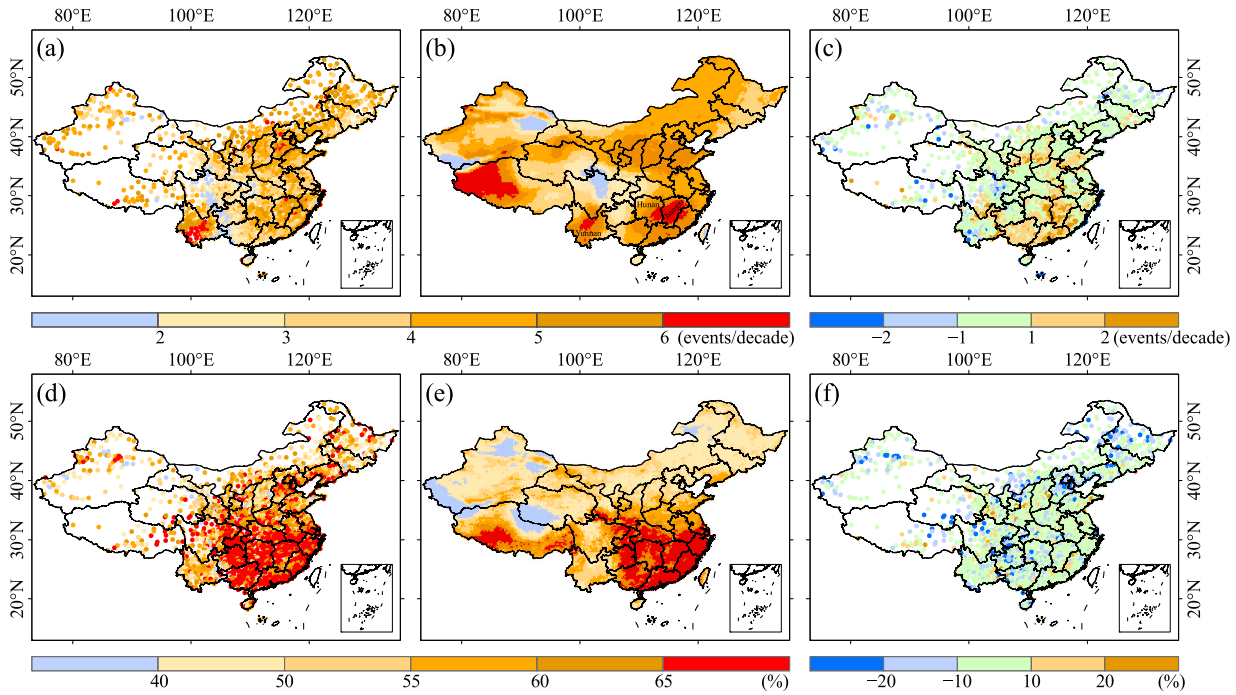

Fig. 2. Spatial distributions of flash drought frequencies based on (a) observations (seven PET methods) during 1981–2020, (b) 24 model-ensemble mean (TH69 PET method) of NEX-GDDP-CMIP6 during 1981–2014, and (c) their absolute differences (simulations minus observations). (d–f) The same as Fig. 2a–c, but for the mean proportion of Case 4 events to all events in the historical period.

emission scenarios (Supplementary Materials, Figs. S9 and S10). Overall, flash droughts will have an extended range of onset dates within the year due to an increase in the frequency of flash droughts under global warming. The magnitude of this effect increases with higher levels of warming, leading to more pronounced shifts in the timing of the first and last flash drought events.

3.3. Future changes of flash droughts

We further investigated changes in flash droughts under the two future scenarios. Flash drought frequencies in China exhibited significant upward trends during 2015–2100 under both SSP scenarios (Fig. 5a), with trends of 0.029 events/decade under SSP245 and 0.067 events/decade under SSP585. The increase rate of flash drought frequency under SSP585 scenario was about 1.3 times higher than that under SSP245. Similarly, the proportions of Case 4 flash drought events to the total events also showed significant upward trends during 2015–2100 (Fig. 5b), with increase rates of 0.691 %/decade under SSP245 and 1.287 %/decade under SSP585. We abstracted three equivalent time periods to analyze future flash drought changes: historical reference period (1981–2014), near-future period (2032–2065), and far-future period (2066–2099). The future change is expressed here as the difference between the near/far future frequency (events) and the historical frequency, then divided by the historical frequency. The increments of flash drought frequencies in China during 2032–2065 and 2066–2099, compared to 1981–2014, were 39.38 % (Fig. 5c) and 66.24 % (Fig. 5d), respectively, with regions experiencing the largest increments primarily located in the central regions of China. The proportion increments of Case 4 flash droughts in China during 2032–2065 and 2066–2099, compared to 1981–2014, were 63.86 % (Fig. 5e) and 100.62 % (Fig. 5f), respectively, with regions showing significant increments also concentrated in central China. The spatial patterns of frequency increments in flash droughts were similar in SSP585 compared to SSP245, but with larger increase values of 43.99 % (Fig. 5g) during 2032–2065 and 115.5 % (Fig. 5h) during 2066–2099. The spatial characteristics of proportion increments in Case 4 flash droughts under SSP585 were also similar to those under SSP245, with larger increase values of 73.93 % (Fig. 5i) during 2032–2065 and 184.74 % (Fig. 5j) during 2066–2099.

In general, the frequency increments of flash droughts were more pronounced during 2066–2099 compared to 2032–2065, relative to 1981–2014 under both SSP scenarios. The highest increments were found in central parts of China, reaching up to approximately 150 %. Taking the spatial frequency changes of flash droughts during 2066–2099 under the SSP585 scenario as an example, we found that most models were able to simulate the spatial frequencies of significant increases in future flash droughts compared to historical period (Fig. 6), particularly in the central parts of China. The spatial proportion increases of Case 4 flash droughts under both SSP scenarios were similar to those of the total frequency, but with further increases. Overall, future flash drought frequencies show clear increasing trends and the rapidity of these events appear to intensify over time. The magnitude of the increase also grows more pronounced with higher levels of warming.

3.4. Associations between flash droughts and CMEs

We investigated the temporal evolutions of meteorological and SM variables to more clearly understand the mechanisms of flash droughts. Strong below-normal water quantity (P, PWD, and SM) and above-normal evapotranspiration capacity (PET, T_{max}, and VPD) were observed during flash droughts (Fig. 7). PWD fell rapidly about 1–2 pentads and 2–3 pentads ahead of surface and root-zone SM. PWD decreased slightly more rapidly and its negative peak was more pronounced compared to SM. Positive evapotranspiration capacity was maintained for about 7 pentads, allowing the PWD below the 20th percentile to be maintained for about 7 pentads (i.e., the duration of a flash drought). The average durations of flash droughts were calculated by dividing the total durations by the total frequencies. The average duration of a flash drought was around 6–6.6 pentads in the observations, while the uncertainty range of MME was slightly larger than the observations, with durations of around 6.4–7.3 pentads in the historical period (Fig. 8). Although the MME slightly overestimated flash drought

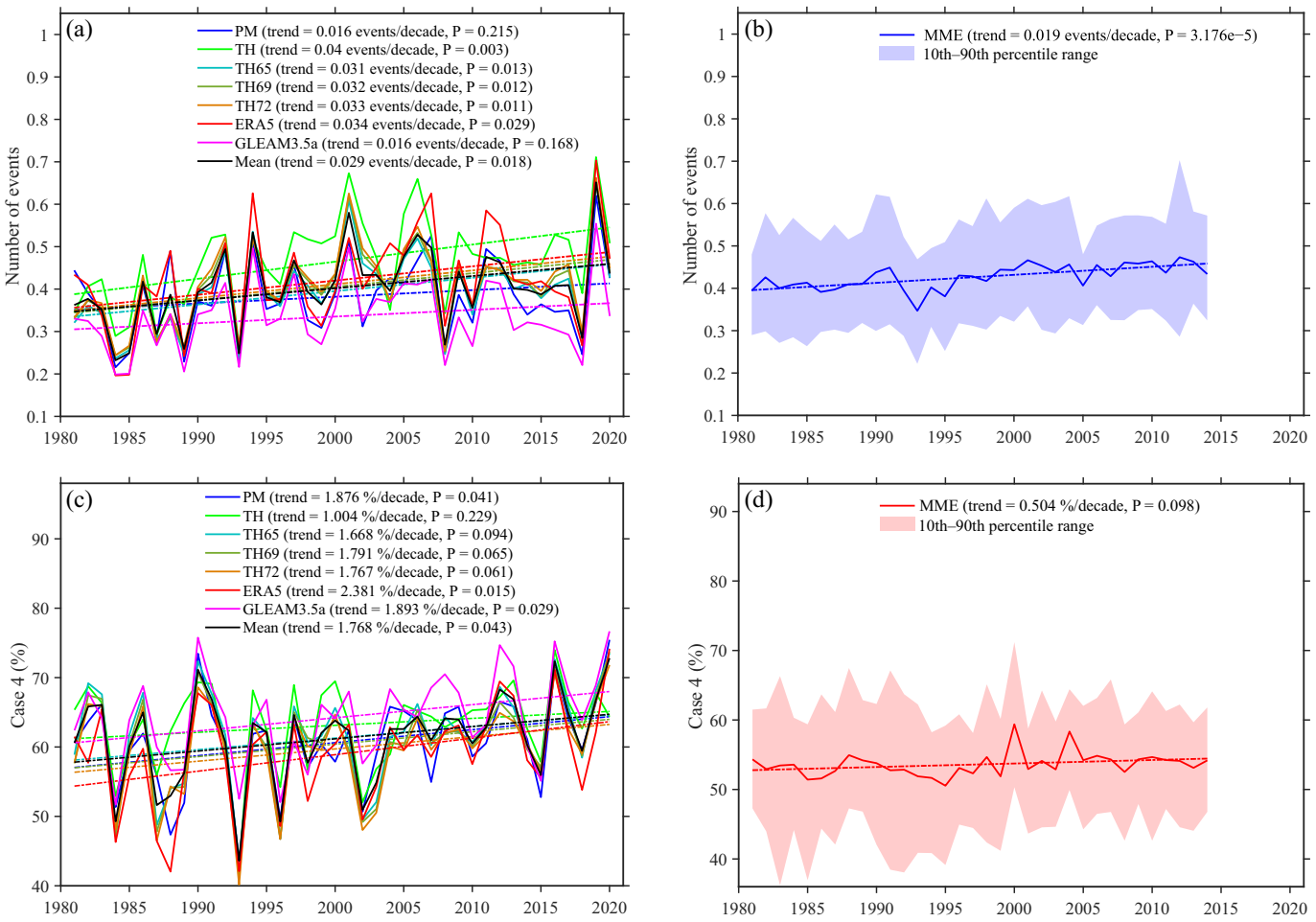

Fig. 3. Annual frequencies of flash droughts based on (a) observations (seven PET methods) during 1981–2020 and (b) 24 model-ensemble mean (TH69 PET method) of NEX-GDDP-CMIP6 during 1981–2014. (c–d) The same as Figs. 2a–b, but for mean proportion of Case 4 events to all events in historical period.

duration by about 0.5 pentads, the model simulations reasonably reflected flash drought duration on the whole.

High evapotranspiration capacity corresponds to low PWD during flash droughts. We applied different combinations of the three variables (T_{max}, VPD, and Wind) representing evapotranspiration capacity to investigate the probability of evapotranspiration-related CMEs during flash droughts, which was used to represent the impact of CMEs on flash droughts. As shown in Fig. 9, high proportions of the four types of CMEs were predominantly located in the southern parts of China, including Jiangxi, Hunan, and Yunnan provinces. This suggests that CMEs in southern China are prone to inducing flash droughts. The spatial proportions of MME aligned closely with observations, suggesting that models reflected proportion patterns of flash droughts induced by CMEs and offered reliable insights into future proportion changes.

To further quantify the proportion patterns of the four types of CMEs that induce flash droughts, we investigated their proportions during flash droughts on the valid stations/grids with threshold values of 1 %, 10 %, and 20 %. As the proportion threshold increased, the probability of CME-induced flash drought events became more pronounced (Fig. 10). For instance, when the proportion threshold of CMEs during flash droughts exceeded 20 %, the proportions of flash droughts induced by compound T_{max} & VPD & Wind events (around 35 % in observations and 31 % in MME) were significantly higher than those induced by other CMEs. The model-simulated proportions of flash droughts induced by CMEs generally aligned with the observations, although the MME slightly underestimated the proportion. Overall, compound T_{max} & VPD & Wind events exhibit a high propensity for triggering flash droughts.

The probabilities (proportions) of CMEs triggering flash droughts appear to increase in the future (Fig. 11). The largest increases are expected in the proportions of compound T_{max} & VPD events. Under the SSP245 scenario, the median increments of proportions of compound T_{max} & VPD events during flash droughts for the near- and far-future were found to be 11.3 % and 10.8 %, respectively. Under the SSP585 scenario, the median increments of proportions of compound T_{max} & VPD events during flash droughts for the near- and far-future are 14.7 % and 25.1 %, respectively. These substantial increases in the far-future proportions of flash droughts induced by CMEs are particularly intense under high emission scenarios, such as the SSP585 scenario for 2066–2099. These findings suggest that the likelihood of CMEs triggering flash droughts will become greater as the magnitude of warming increases. The proportional increases in compound T_{max} & VPD events are much larger than those of other compound events, which suggests that the simultaneous occurrence of high temperatures and atmospheric dryness will increase the probability of flash droughts in the future.

4. Discussion

Differences in PET results can arise from the use of different methods or datasets. Our findings align with previously publications (Chang et al., 2019; Trajkovic et al., 2019), showing that PET estimated by the TH65 and TH69 methods closely approximates PM-based results in China. These methods provide an effective alternative for estimating short-term PET, as they require fewer variables compared to PM methods. Notably, indicators such as VPD and PWD exhibit stronger

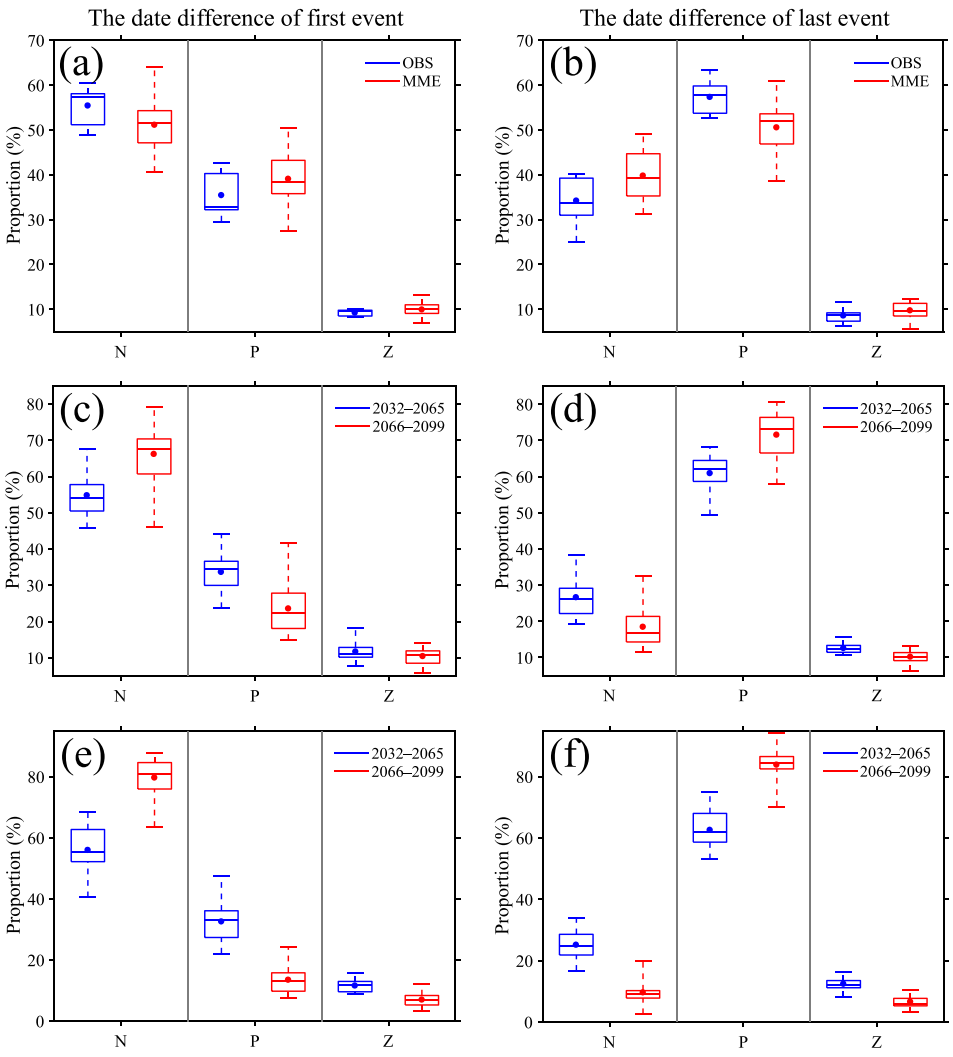

Fig. 4. Proportional characteristics of onset date differences in flash drought events across China. (a) Onset dates (1–73 pentads per year) of the first flash drought event between later and earlier periods in observations (model simulations) during the historical period, (b) the same as Fig. 4a, but for the last flash drought event. (c) Onset date difference in the first flash drought event between 2032–2065 (2066–2099) under the SSP245 scenario and 1981–2014, (d) the same as Fig. 4c, but for the last flash drought event. (e) Onset date difference in the first flash drought event between 2032–2065 (2066–2099) under the SSP585 scenario and 1981–2014, (f) the same as Fig. 4e, but for the last flash drought event. The MME in the historical period is based on the TH69 PET method, which denotes the onset date difference of the first flash drought event during 1998–2014 and 1981–1997. The OBS in the historical period is the observed value based on averages of the seven PET methods for the date of the first flash drought event during 2001–2020 minus the date of 1981–2000. N denotes a negative value, indicating that the onset date of the flash drought event will be earlier in the later period than in the earlier period. P denotes a positive value, where the onset date of the flash drought event will be later in the later period than in the earlier period. Z denotes a zero value, where there is no change in the onset date of the flash drought event between the later and earlier periods.

associations with flash droughts than temperature and precipitation (Ford and Labosier, 2017; Qing et al., 2022). Consequently, spatial distributions of flash droughts identified using PWD may be similar to those identified using the ESR method (Christian et al., 2021), both of which are based on meteorological perspectives. To assess PWD-derived flash droughts, we evaluated satellite data, reanalysis data, and model simulations of SM. The PWD-derived flash droughts in this study were primarily based on a meteorological perspective and can be referred to as "meteorological flash droughts". SM is the critical hydroclimatic variable that directly determines the severity and effects of flash droughts, such as vegetation stress (O and Park, 2023; Yuan et al., 2019). While PWD indirectly affects SM through its influence on precipitation and PET, examining SM directly provides useful insights into the extent of land-surface desiccation associated with PWD-derived flash droughts. As shown in Fig. 12, the average surface SM percentiles during the last three pentads of PWD-derived flash droughts were depleted to below 20 %, with even lower values (< 10 %) in southern areas. The average RI decline in surface SM was generally >5 %/pentad, reaching as high as 15 %/pentad in eastern regions. The surface SM exhibited a lag time of 1–2 pentads behind PWD, indicating a relatively faster response of surface SM to PWD. As shown in Fig. 13, the average percentiles of root-zone SM (0–100 cm) during the last three pentads of PWD-derived flash droughts were generally higher than the surface SM percentiles. Root-zone SM percentiles dropped below 20 % in most areas, especially in certain southern parts of China (generally below 15 %). The rate of decline in root-zone SM reached 5 %/pentad and was especially intense in the Yangtze River basin (around 10 %/pentad). The lag time of root-zone SM was longer than that of surface SM and was longer in the south than the north. This disparity may be attributable to the abundance of water resources in southern China. In these areas, precipitation deficits and strong evapotranspiration need to persist for a longer duration before the root-zone SM reaches a dry state. Notably, the PWD-derived flash drought signal exhibited greater prominence in surface SM than root-zone SM, indicating that deep SM has a stronger memory than near-

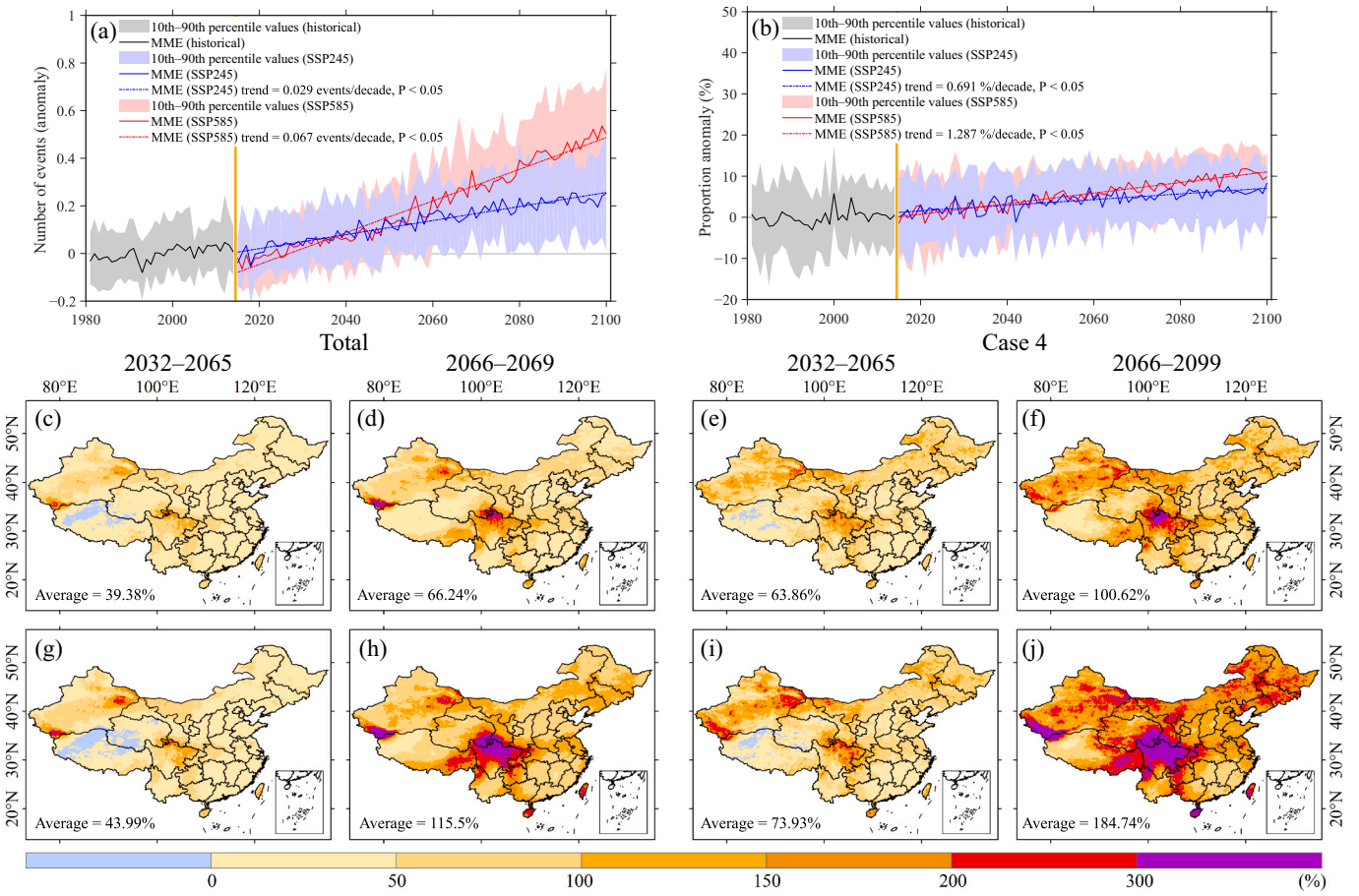

Fig. 5. Annual changes in flash drought frequency under SSP245 and SSP585 scenarios. (a) Annual frequency anomalies in flash droughts. (b) Annual anomalies in proportions of Case 4 flash drought events to all events. Spatial frequency changes of flash droughts during (c) 2032–2065 and (d) 2066–2099 compared to 1981–2014 under SSP245 scenario. Spatial changes in proportions of Case 4 flash drought events to all events during (e) 2032–2065 and (f) 2066–2099 compared to 1981–2014 under SSP245 scenario. Spatial frequency changes in flash droughts during (g) 2032–2065 and (h) 2066–2099 compared to 1981–2014 under SSP585 scenario. Spatial changes in proportions of Case 4 flash drought events to all events during (i) 2032–2065 and (j) 2066–2099 compared to 1981–2014 under SSP585 scenario.

surface meteorological variables, resulting in a slower development of drought conditions. Overall, the PWD-derived flash droughts can effectively capture the sharp intensification of drought conditions leading to depleted SM and associated drought effects.

Additionally, the standardized precipitation evapotranspiration index (SPEI) reflects atmospheric evaporative demand and can be used to identify flash droughts on short timescales, typically less than one month. This can provide for early warning signals of SM-derived flash droughts (Noguera et al., 2020; Tian et al., 2020). We calculated SPEI using the difference between observed precipitation and PM PET (pentad PWD) to further evaluate the suitability of PWD in identifying flash droughts. When setting the PWD to the 20th percentile, the average SPEI value in China was −0.8 (Fig. 14a), indicating moderate drought conditions. When PWD was set to the 40th percentile, the average SPEI value in China was −0.2 (Fig. 14b), indicating aridification tendencies. To establish a correspondence between PWD-derived and SPEI-derived flash droughts, we replaced the important PWD threshold values of the 40th and 20th percentiles with −0.2 and −0.8, respectively, for SPEI-derived flash droughts. There were more SPEI-derived flash droughts in the northern, southeastern, and southwestern parts of China (Fig. 14c), reaching a frequency of 5 events/decade. This pattern can be attributed to the lower SPEI values (below −0.8) in the north at the 20th PWD percentile threshold, leading to more lenient conditions for identifying flash droughts and resulting in a higher frequency. Case 4 flash droughts accounted for 70 % of the events in the southern parts of China (Fig. 14d). We found that the spatial frequency patterns identified by these two methods were largely similar, although the SPEI-derived flash droughts in northern China were significantly higher than that of PWD-derived flash droughts. This divergence may be attributable to the suitability of SPEI in different climatic areas. The wide expanse of semi-arid and arid areas in northern China may have led to unrealistic SPEI values, as PWD may not conform to the logistic distribution (Vicente-Serrano et al., 2010).

The observations revealed hotspot areas of PWD-derived flash droughts in northern, southwestern, and southeastern parts of China. These spatial characteristics were consistent with ESR-based flash drought studies (Christian et al., 2021; Gong et al., 2022), likely because both ESR and PWD capture atmospheric evaporation demand signals. The southern parts of China exhibited faster onset speeds of flash droughts, as indicated by higher proportions of Case 4 flash droughts (i.e., one-pentad onset time) in this study. This finding aligns with previous research by Yuan et al. (2023), who suggested that relatively wet areas capable of experiencing large precipitation deficits and evapotranspiration can accelerate SM desiccation, leading to more flash droughts. We found an evident upward trend in the proportion of Case 4 flash droughts, which aligns with a previous analysis based on the onset speeds of SM-derived flash droughts (Qing et al., 2022). PWD-derived flash drought frequencies showed significant upward trends under both future SSP scenarios, which align closely with the meteorological characteristics of flash droughts identified by 12 global climate models

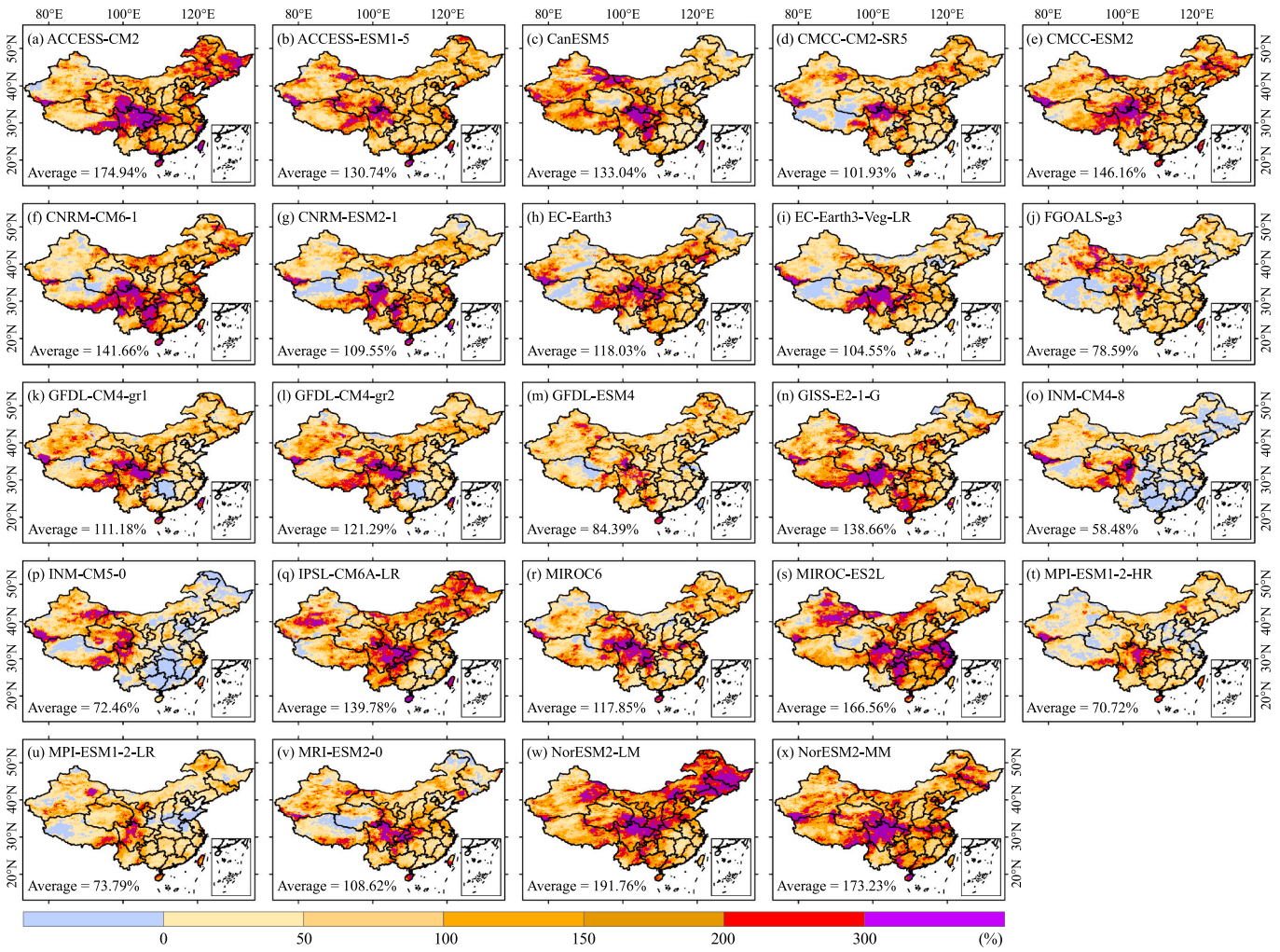

Fig. 6. Spatial frequency changes in flash droughts based on model simulations during 2066–2099 under SSP585 scenarios compared to 1981–2014 (historical reference period).

(Sreeparvathy and Srinivas, 2022). Similarly, in India, the frequency of SM-derived (0–60 cm) flash droughts is projected to increase due to the interseasonal variability of summer monsoon precipitation and anthropogenic warming (Mishra et al., 2021). The proportions of Case 4 flash droughts show significant upward trends in both future scenarios, suggesting that future flash droughts will come on faster. This result is consistent with previous findings regarding SM-derived flash droughts (Yuan et al., 2023), which may be attributed to amplified evapotranspiration anomalies and precipitation deficits. The spatial characteristics of the Case 4 flash droughts are similar to those of overall flash drought frequency in the future, with Case 4 events increasing more rapidly, particularly in central and northern regions of China. This indicates a growing contribution of flash droughts occurring within one-pentad time to the total flash droughts.

The lengths of the annual four seasons in China have changed significantly due to global warming. Spring and summer now begin significantly earlier, while autumn and winter are significantly delayed (Chen et al., 2023b). These changes have impacted the annual occurrence dates of heat-related extreme events such as droughts and heatwaves (Mo, 2011; Shi et al., 2021). Urbanization may accelerate the onset of heat waves (Luo and Lau, 2017), potentially influencing the onset dates of flash droughts. Flash droughts tend to occur in the summer due to precipitation deficits and sudden increases in evapotranspiration capacity, which can have drastic economic effects. For example, a flash drought event in Russia during the summer of 2010 led to a decline in wheat yields of >70 % in top wheat-producing oblasts, which led to a large drop in global wheat stocks and a rapid increase in wheat prices across the globe (Hunt et al., 2021). Flash droughts can also trigger other natural disasters, such as forest fires and air pollution. If a flash drought occurs in early spring, it can affect crop planting and lead to crop failure (Haslinger and Mayer, 2023). Severe spring droughts negatively affect the radial growth of forest trees, reducing crown density and the formation of female cones (Thabeet et al., 2009). A flash drought occurring in late autumn makes the area susceptible to winter droughts, which affect the wood structure of forests and can easily lead to xylem embolism (Camarero et al., 2016). A flash drought in late autumn may also evolve into a winter-spring drought, delaying the start of the vegetation growing season. Zhang et al. (2023a) utilized reanalysis data SM during 1981–2021 to conclude that the frequencies and durations of flash droughts have intensified in China during the spring and autumn months. The timing of the onset of flash drought plays an important role in crops, ecosystems, and socio-economics (Hunt et al., 2021). Presently, there is limited research on such timing of flash droughts onset dates in terms of both observational and downscaled model simulations. In this study, we found that the onset date of the first PWD-derived flash drought will likely occur earlier under global warming, while the onset date of the last flash drought may come later, particularly under high-emissions scenarios in the far-future.

The frequency of heat-related compound events is increasing under climate warming, further elevating the likelihood of flash droughts,

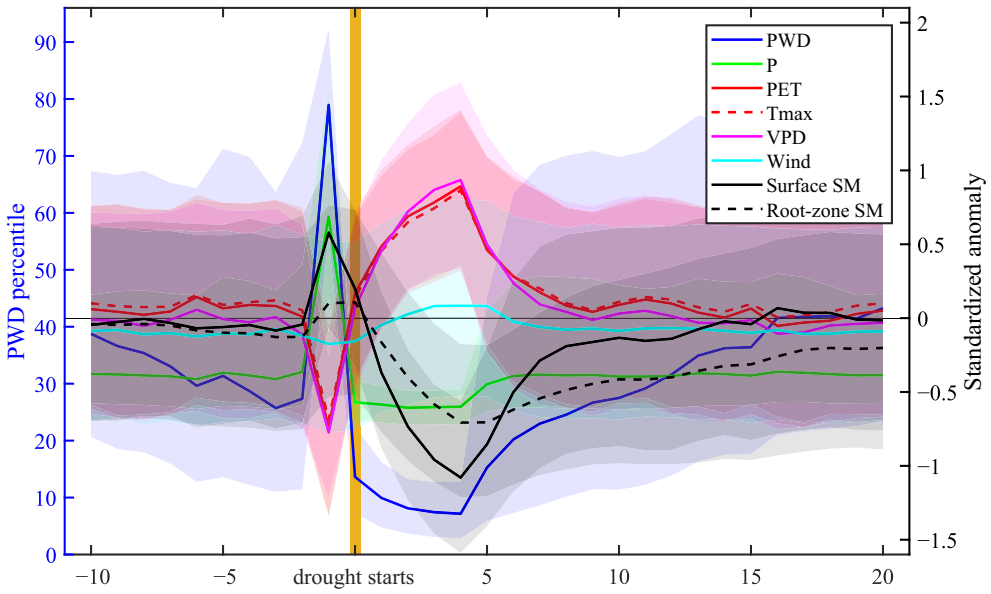

Fig. 7. Temporal evolution of meteorological and SM variables during flash droughts across China during 1981–2020. The left y-axis represents the PWD percentile and the right y-axis represents the standardized anomalies of the meteorological variables and SM. Lines indicate medians and shading indicates the interquartile range. The number of flash droughts at a grid level is 37,454. Meteorological variables are station observations. PET calculation is based on the TH69 method. SM was derived from the ERA5 dataset for the surface layer (0–7 cm) and root zone (0–100 cm), respectively.

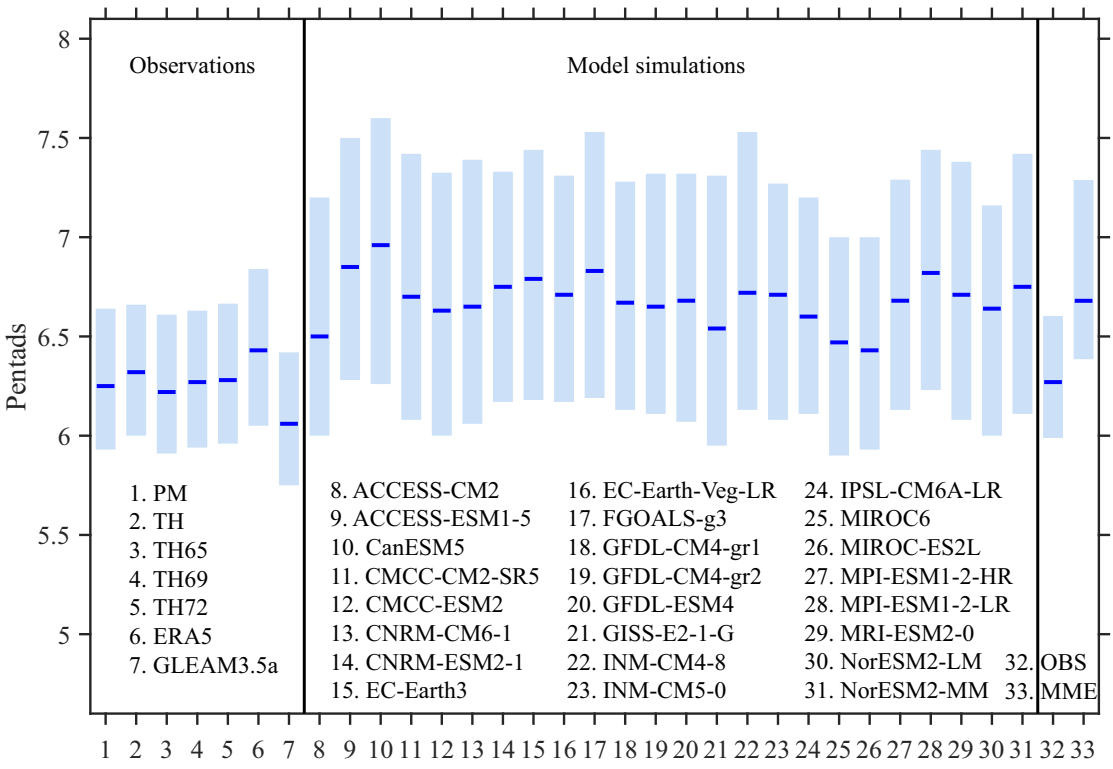

Fig. 8. Mean durations of flash droughts based on observations and 24 model simulations during historical period. Light-blue box indicates the interquartile range, and blue line marks the median value.

particularly in the far-future under SSP585 (Mishra et al., 2021; Ridder et al., 2020; Yin et al., 2023; Yu and Zhai, 2020; Zhang et al., 2020b; Zhou et al., 2019). High temperatures and precipitation deficits contribute to elevated VPD, which intensifies atmospheric dryness and accelerates SM depletion, ultimately leading to flash droughts (Christian et al., 2021; Qing et al., 2022; Zhang et al., 2017). VPD plays an important role in the rapid onset of droughts (Qing et al., 2022), making it a key factor in flash drought development. Therefore, CMEs involving VPD (e.g., compound T_{max} & VPD & Wind events) have a high probability of triggering flash droughts (Supplementary Materials, Fig. S11). Land-atmosphere coupling, influenced by prolonged SM deficits transitioning from latent heat to sensible heat, can intensify surface warming and induce anomalous anticyclonic circulation patterns, thus amplifying heatwaves and exacerbating soil dryness (Zhang et al., 2020a), thereby

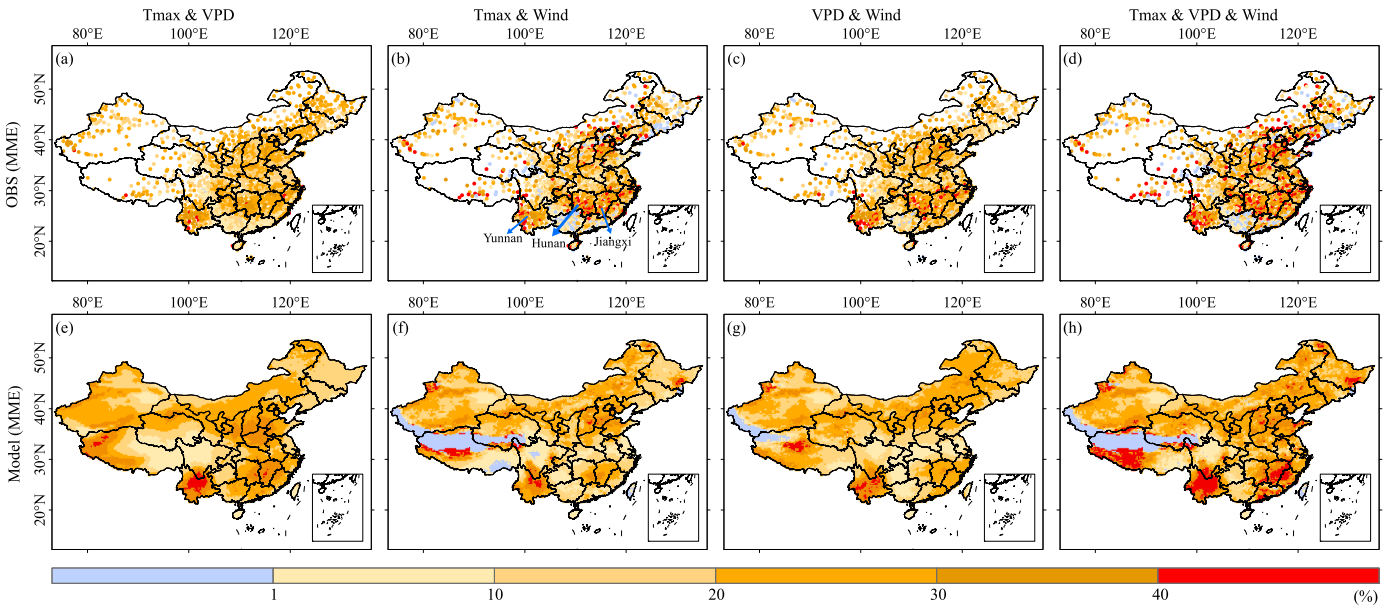

Fig. 9. Associations between flash droughts and CMEs. Proportions of (a) compound T_{max} & VPD events, (b) compound T_{max} & Wind events, (c) compound VPD & Wind events, (d) compound T_{max} & VPD & Wind events occurring within flash droughts based on averages of seven PET observations during 1981–2020. (e–h) The same as Fig. 9a–d, but for MME during the historical period (1981–2014).

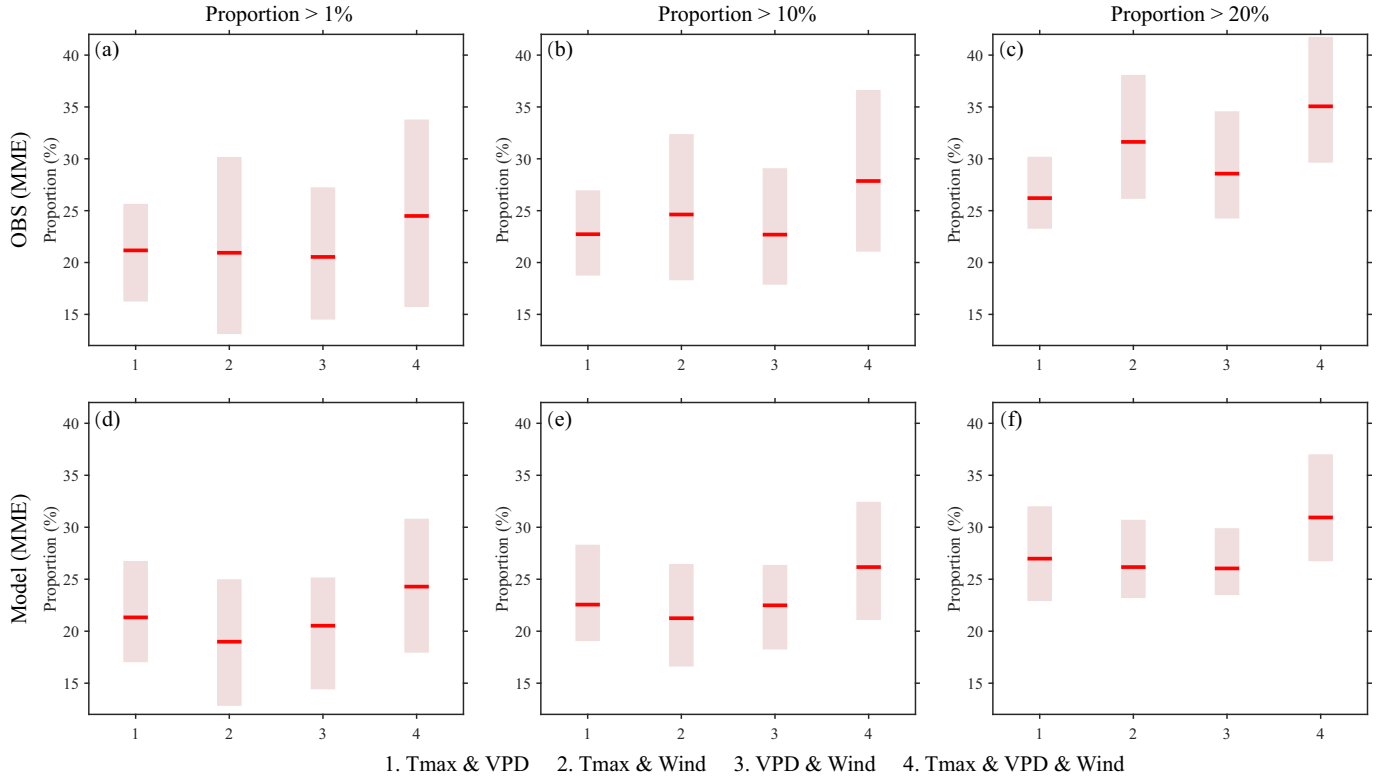

Fig. 10. Interquartile ranges (box) of four types of CMEs >1 %, 10 %, and 20 % simultaneously during flash droughts at the same stations/grids based on (a–c) multi-observations and (d–f) MME during the historical period (observation: 1981–2020, model: 1981–2014). Red lines indicate medians of proportions on stations/grids.

increasing the severity of flash droughts. Flash droughts, due to their coincidence with dryness-related CMEs, have a more pronounced impact on agricultural activities and ecological safety than single-type droughts (Mahto and Mishra, 2023; Mohammadi et al., 2022). Future warming will increase the risk of compound drought and heatwave events (Tripathy et al., 2023). The probability of such compound extremes (i.e., the compound T_{max} & VPD events described in this study) triggering flash droughts will increase in the future as well, although there are differences in the spatial proportion changes among the models in the far-future under SSP585 scenario (Fig. 15). The spatial proportion changes of compound T_{max} & VPD events in far-future under SSP585 scenario are better able to account for overall changes in far-future flash droughts under SSP585 scenario. During crop-growing seasons, flash droughts are typically triggered by compound hot and dry conditions

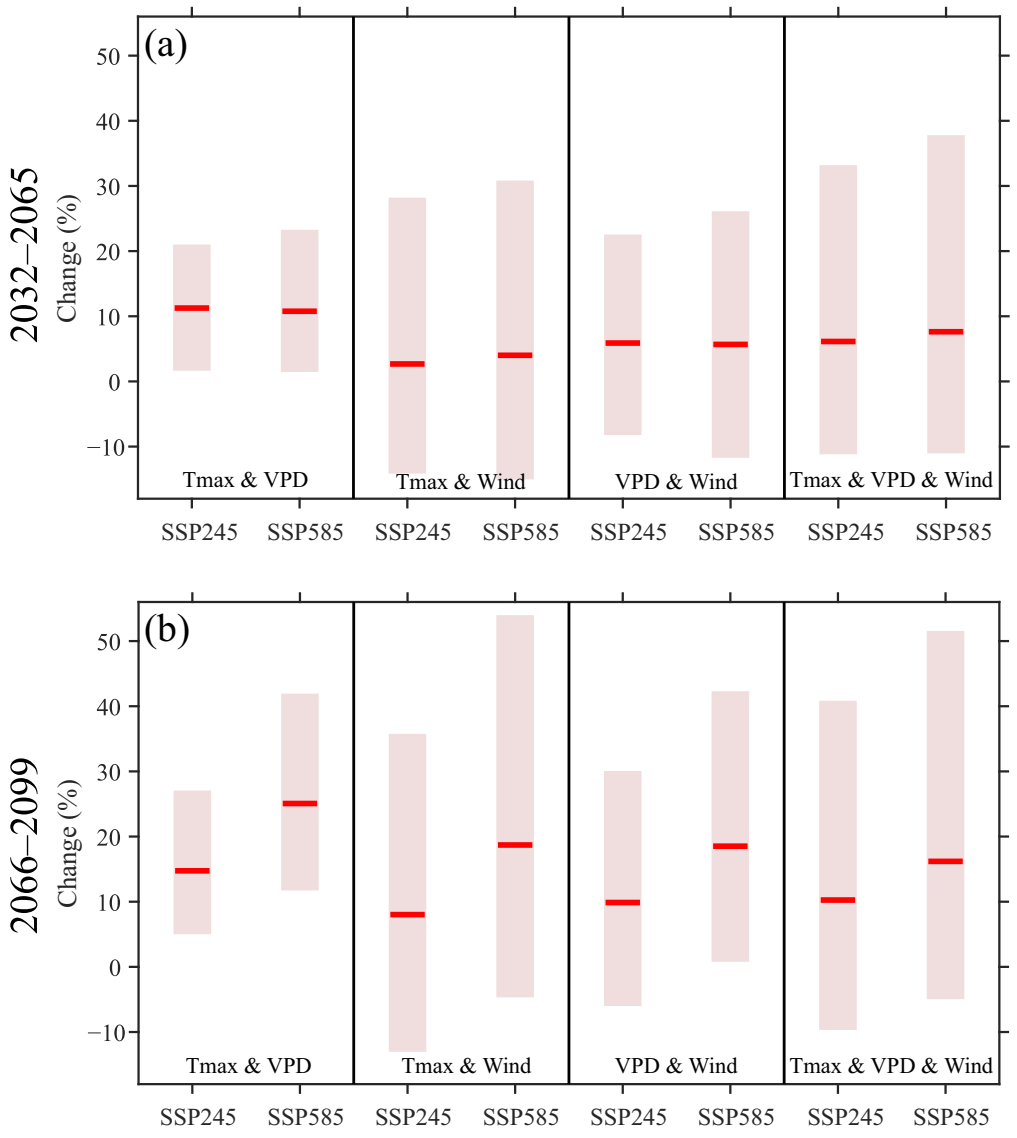

Fig. 11. Projected changes in CME proportions during flash droughts based on 24-model-ensemble means for (a) 2032–2065 and (b) 2066–2099 under SSP245 and SSP585 scenarios, respectively (reference period: 1981–2014). Light-red box indicates the interquartile range, and red line marks the median value.

leading to a sharp decline in SM (Mishra et al., 2021; Qing et al., 2022). Low SM may also contribute to compound hot and dry extremes and other dryness-related CMEs through strong land-atmosphere interactions, thereby amplifying the severity of extreme events (Hao et al., 2022; Zhang et al., 2020a; Zhou et al., 2019; Zscheischler et al., 2020). Flash droughts in Russia in June of 2010 were followed by compound heatwaves and atmospheric drying events during the subsequent drought phase, illustrating the interconnectedness of these phenomena through land-atmosphere interactions (Christian et al., 2020). Future research could explore the feedback of flash droughts on CMEs in terms of land-atmosphere effects in high-resolution observations and model simulations.

The spatial patterns and long-term trends of flash droughts identified from atmospheric evaporation demand and SM perspectives may differ due to the inherent characteristics of meteorological and subsurface variables. To construct comprehensive flash drought indicators, it may be effective to integrate atmospheric evaporation demand, SM, and even vegetation indices (e.g., chlorophyll fluorescence, leaf area index, and vegetation health index) (Mohammadi et al., 2022; Sun et al., 2022; Wang et al., 2023a). SM-derived (root-zone) flash droughts are not increasing in many areas worldwide, but have intensified at a faster rate in recent decades (Qing et al., 2022). This phenomenon contrasts with the increasing trend in the frequency of flash droughts in our study. The disparity may be attributable to the differences in methodology for defining the percentiles of SM and PWD. Mukherjee and Mishra (2022) pointed out that differences in the features identified by different flash drought methods and data sources, i.e., the uncertainties of flash droughts are driven by the choice of methodology and differences in input data. Although there is relative consistency in the characteristics of historical flash drought based on the observations, satellite remote sensing, and reanalysis data in this study, the variability of model simulations may have created inconsistencies in the identified flash droughts, especially under different future emission scenarios. Although the NEX-GDDP-CMIP6 datasets were generated by the latest global meteorological forcing dataset (integration of reanalysis data and observations) and BCSD downscaling method, the downscaled values corresponding to extreme events in some areas may have been underestimated due to the translation of the data from low to high spatial resolution (Thrasher et al., 2022; Zhang et al., 2023b). These errors in extreme values have the potential to be magnified in the future, thus increasing the uncertainties of flash droughts.

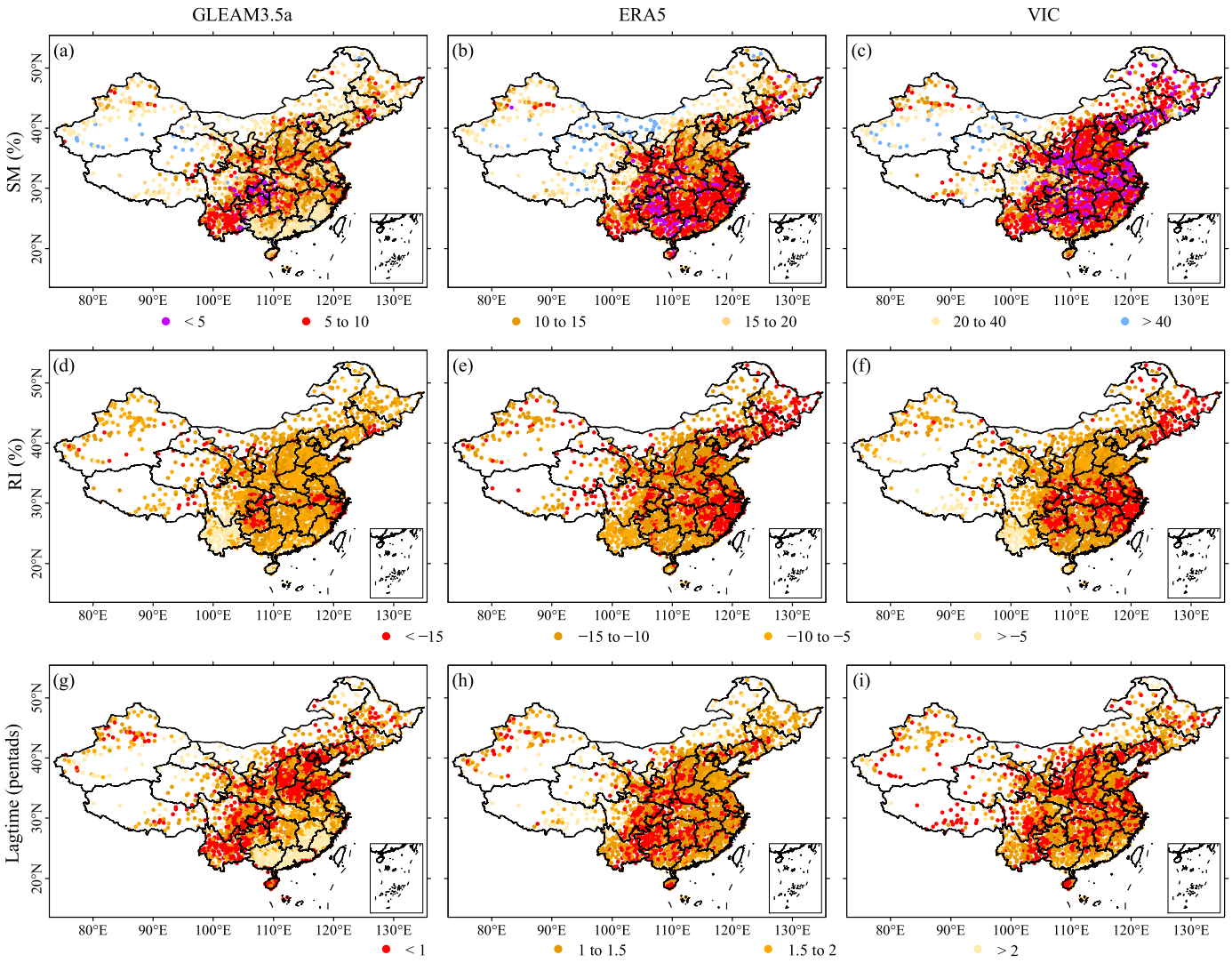

Fig. 12. Surface SM characteristics under flash drought conditions based on PWD. (a–c) Mean SM percentile in last three pentads of flash droughts, (d–f) RI of mean SM (pentad when SM is first ≤20th percentile, forward to other 3 pentads under PWD flash droughts), and (g–i) number of pentads where SM lags behind PWD (difference between pentads of first PWD ≤ 20 % and first SM ≤ 20 % under PWD flash droughts). Precipitation observations and each PET dataset used to calculate PWD, where PET in VIC is based on PM method of observations. Surface depths of GLEAM3.5a, ERA5, and VIC are 0–10 cm, 0–7 cm, and 0–10 cm, respectively.

5. Conclusions

As hot-dry compound extremes become more frequent with climate warming, the probability of flash droughts with rapid onset speeds is anticipated to increase. These changes in flash droughts are expected to further exacerbate agricultural, environmental, and socio-economic impacts, potentially triggering subsequent disasters. In this study, we investigated PWD-derived flash droughts and their relationship with CMEs in China based on observations and 24 downscaled CMIP6 simulations in historical and future periods. Our findings can be summarized as follows.

(1) NEX-GDDP-CMIP6 can reasonably reflect the spatial characteristics and long-term trend characteristics of P − PET, which in turn can reasonably reflect the spatial and temporal characteristics of PWD-derived flash droughts. Historical flash drought hotspots were concentrated in the northern and southern parts of China. Large proportions of Case 4 (i.e., one-pentad onset time) events in the total frequency of flash droughts were mainly concentrated in the southern parts of China, which indicated that flash droughts occurred most rapidly in these regions. Pronounced upward trends in the frequencies of flash droughts across China in both observations and model simulations may be attributable to increased frequencies of the most rapidly occurring events in the historical period.

(2) The onset dates of the first and last flash droughts throughout the year are expected to shift earlier and later, respectively, thus expanding the onset dates of flash droughts both in the observations and model simulations in the historical period. The first flash drought event will occur earlier and the last flash drought event will occur later for the vast majority of China in the far-future under high-emission scenarios, which will increase the likelihood of advanced or delayed occurrence for the flash drought events. The magnitude of this effect intensifies with higher levels of warming, leading to more pronounced shifts in the timing of the year's first and last flash drought events.

(3) Flash drought frequencies exhibited significant upward trends under both future SSP scenarios, particularly SSP585. The proportions of Case 4 flash droughts showed significant upward trends in both future scenarios, suggesting a faster onset of future flash droughts. The spatial characteristics of Case 4 flash droughts closely resemble those of overall flash drought frequency in the future, with Case 4 events increasing more rapidly, particularly in central regions of China. This indicates a growing contribution of flash droughts occurring within one-pentad time to the total flash droughts, especially in the far-future under high-emissions scenarios.

(4) A strong association was observed between high T_{max} (PET), high

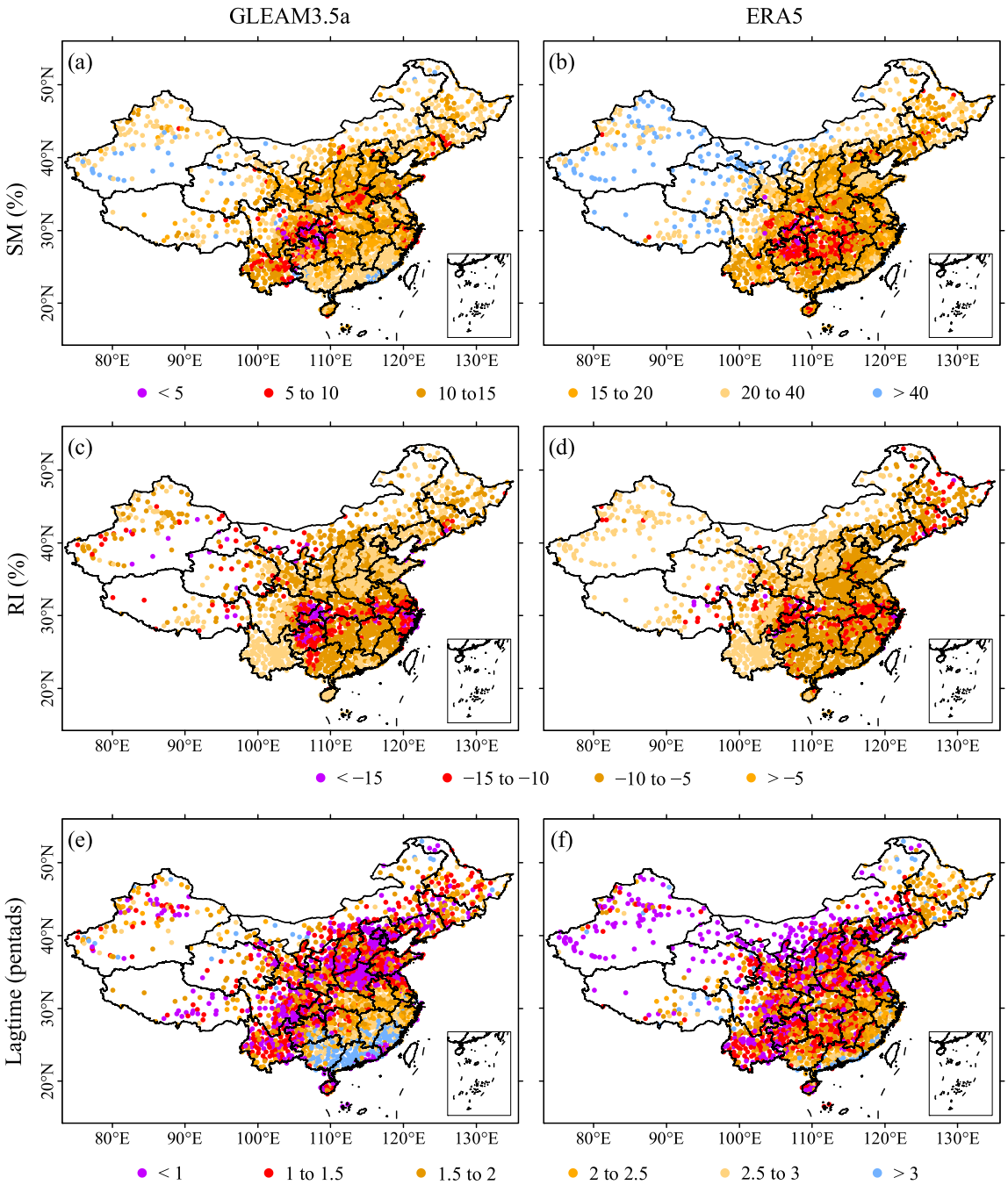

Fig. 13. The same as Fig. 12, but for root-zone SM (0–100 cm) in GLEAM3.5a and ERA5 datasets.

VPD, and strong winds with high flash drought occurrence probability, particularly in southern regions of China. PWD-derived flash droughts effectively capture the sharp intensification of drought conditions leading to depleted SM and associated drought effects. This is due to the PWD falling rapidly about 1–2 pentads and 2–3 pentads ahead of surface and root-zone SM values. CMEs in southern China were prone to inducing flash droughts due to elevated proportions of the four types of CMEs. Overall, compound T_{max} & VPD & Wind events presented a high probability for triggering flash droughts. The probability of CMEs triggering flash droughts is expected to increase as the magnitude of warming increases. The proportion increases of compound T_{max} & VPD events will be much larger than those of other compound events, especially in the far-future under the SSP585 scenario.

CRediT authorship contribution statement

Yuqing Zhang: Conceptualization, Data curation, Formal analysis, Funding acquisition, Investigation, Methodology, Validation, Writing – original draft, Writing – review & editing. **Qinglong You:** Conceptualization, Supervision, Visualization, Writing – review & editing. **Changchun Chen:** Supervision, Writing – review & editing. **Huaijun Wang:** Investigation, Software, Validation. **Safi Ullah:** Investigation, Validation. **Liucheng Shen:** Data curation, Visualization.

Declaration of competing interest

The authors declare that they have no known competing financial interests or personal relationships that could have appeared to influence the work reported in this paper.

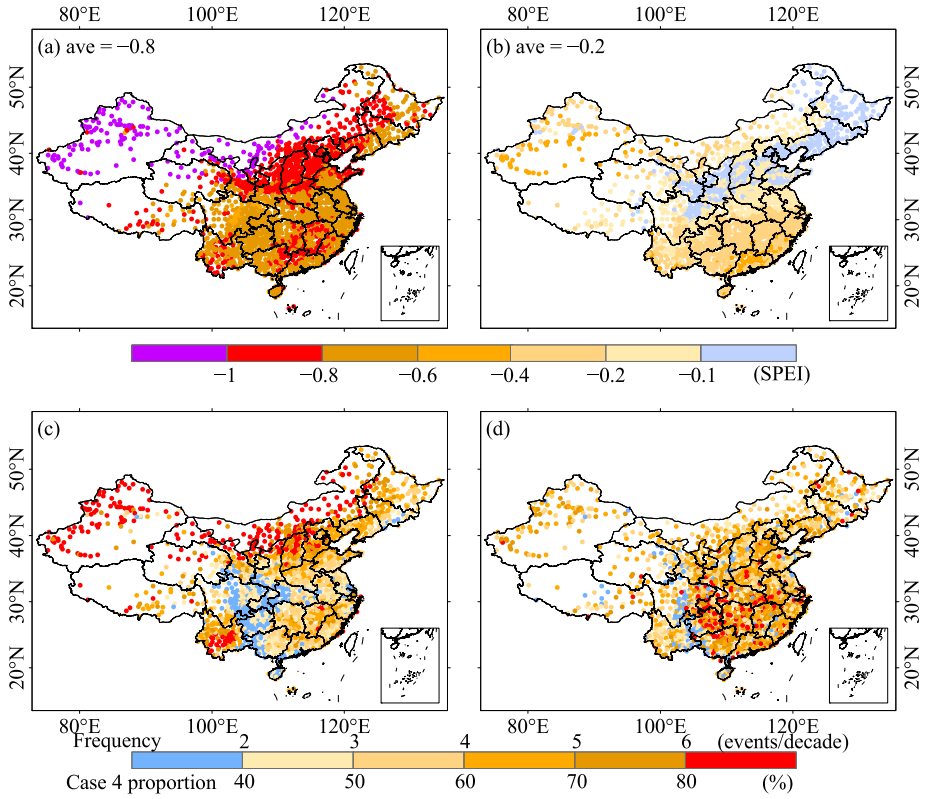

Fig. 14. SPEI values corresponding to (a) 20th and (b) 40th PWD percentiles during 1981–2020 (pentad scale). (c) Frequency of flash droughts and (d) proportion of Case 4 events to total events based on pentad SPEI. SPEI calculated was based on observational precipitation and PM PET.

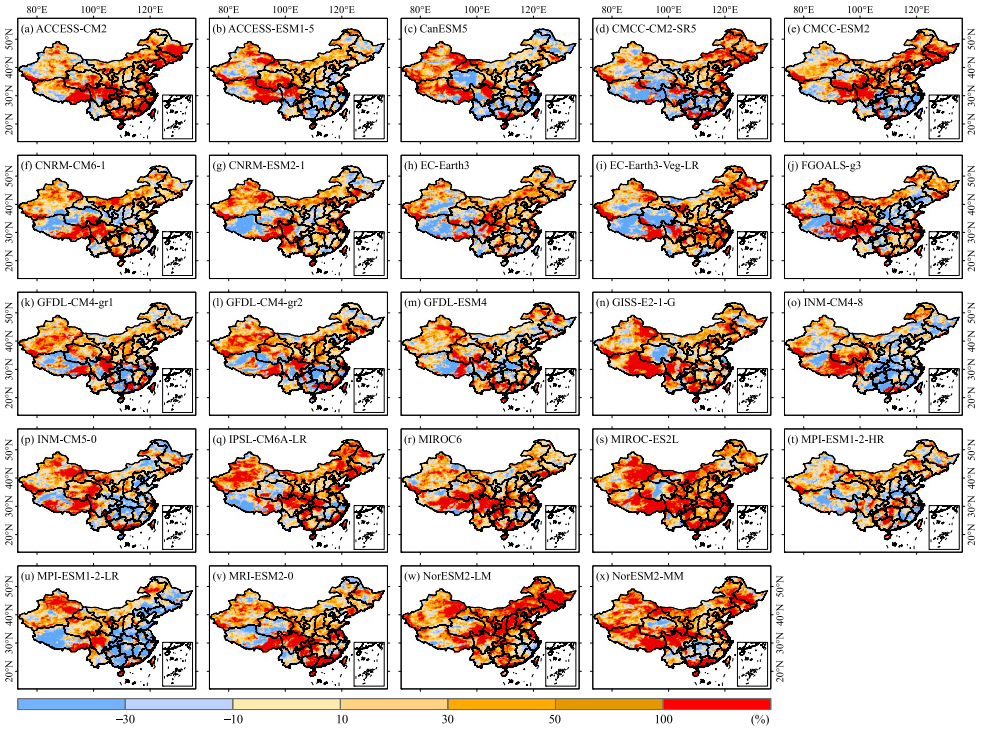

Fig. 15. Spatial proportions changes of compound T_{max} & VPD during flash droughts based on model simulations during 2066–2099 under SSP585 scenarios compared to 1981–2014 (historical reference period).

Data availability

The data that has been used is confidential.

Acknowledgements

This study was jointly supported by the National Natural Science Foundation of China (41907384), the MOE (Ministry of Education in China) Project of Humanities and Social Sciences (19YJCZH259), and the Qinglan Project funded by universities in Jiangsu Province (2023).

Appendix A. Supplementary data

Supplementary data to this article can be found online at https://doi.org/10.1016/j.scitotenv.2024.170133.

References

Allan, R.P., 2023. Amplified seasonal range in precipitation minus evaporation. Environ. Res. Lett. 18, 094004.
Allen, R.G., Pereira, L.S., Raes, D., Smith, M., 1998. Crop evapotranspiration. Guidelines for computing crop water requirements. In: Fao Irrigation & Drainage Paper, p. 56.
Basara, J.B., Christian, J.I., Wakefield, R.A., Otkin, J.A., Hunt, E.H., Brown, D., 2019. The evolution, propagation, and spread of flash drought in the Central United States during 2012. Environ. Res. Lett. 14, 084025.
Camarero, J.J., Guada, G., Sánchez-Salguero, R., Cervantes, E., 2016. Winter drought impairs xylem phenology, anatomy and growth in Mediterranean Scots pine forests. Tree Physiol. 36, 1536–1549.
Chang, X., Wang, S., Gao, Z., Luo, Y., Chen, H., 2019. Forecast of daily reference evapotranspiration using a modified daily thornthwaite equation and temperature forecasts†. Irrig. Drain. 68, 297–317.
Chen, L., Li, Y., Ge, Z.-A., Lu, B., Wang, L., Wei, X., et al., 2023a. Causes of the extreme drought in late Summer–Autumn 2019 in Eastern China and its future risk. J. Clim. 36, 1085–1104.
Chen, Y., Zhang, Y., Li, Y., Song, S., 2023b. Changes in lengths of the four seasons in China and the relationship with changing climate during 1961–2020. Int. J. Climatol. 43, 1349–1366.
Chiang, F., Mazdiyasni, O., AghaKouchak, A., 2018. Amplified warming of droughts in southern United States in observations and model simulations. Sci. Adv. 4, eaat2380.
Christian, J.I., Basara, J.B., Otkin, J.A., Hunt, E.D., 2019. Regional characteristics of flash droughts across the United States. Environ. Res. Commun. 1, 125004.
Christian, J.I., Basara, J.B., Hunt, E.D., Otkin, J.A., Xiao, X., 2020. Flash drought development and cascading impacts associated with the 2010 Russian heatwave. Environ. Res. Lett. 15, 094078.
Christian, J.I., Basara, J.B., Hunt, E.D., Otkin, J.A., Furtado, J.C., Mishra, V., et al., 2021. Global distribution, trends, and drivers of flash drought occurrence. Nat. Commun. 12, 6330.
Di Napoli, C., Barnard, C., Prudhomme, C., Cloke, H.L., Pappenberger, F., 2021. ERA5-HEAT: a global gridded historical dataset of human thermal comfort indices from climate reanalysis. Geosci. Data J. 8, 2–10.
Eyring, V., Bony, S., Meehl, G.A., Senior, C.A., Stevens, B., Stouffer, R.J., et al., 2016. Overview of the Coupled Model Intercomparison Project Phase 6 (CMIP6) experimental design and organization. Geosci. Model Dev. 9, 1937–1958.
Fischer, E.M., Sippel, S., Knutti, R., 2021. Increasing probability of record-shattering climate extremes. Nat. Clim. Chang. 11, 689–695.
Ford, T.W., Labosier, C.F., 2017. Meteorological conditions associated with the onset of flash drought in the Eastern United States. Agric. For. Meteorol. 247, 414–423.
Gong, Z., Zhu, J., Li, T., Huang, D., Chen, X., Zhang, Q., 2022. The features of regional flash droughts in four typical areas over China and the possible mechanisms. Sci. Total Environ. 827, 154217.
Hao, Z., Hao, F., Xia, Y., Feng, S., Sun, C., Zhang, X., et al., 2022. Compound droughts and hot extremes: characteristics, drivers, changes, and impacts. Earth Sci. Rev. 235, 104241.
Haslinger, K., Mayer, K., 2023. Early spring droughts in Central Europe: indications for atmospheric and oceanic drivers. Atmos. Sci. Lett. 24, e1136.
Hersbach, H., Bell, B., Berrisford, P., Hirahara, S., Horányi, A., Muñoz-Sabater, J., et al., 2020. The ERA5 global reanalysis. Q. J. R. Meteorol. Soc. 146, 1999–2049.
Hunt, E., Femia, F., Werrell, C., Christian, J., Otkin, J., Basara, J., et al., 2021. Agricultural and food security impacts from the 2010 Russia flash drought. Weather. Clim. Extremes 34, 100383.
IPCC. Summary for policymakers. In: Climate Change 2021: The Physical Science Basis. Contribution of Working Group I to the Sixth Assessment Report of the Intergovernmental Panel on Climate Change [Masson-Delmotte, V. P Zhai, A. Pirani, S. L. Connors, C. Péan, S. Berger, N. Caud, Y. Chen, L. Goldfarb, M. I. Gomis, M. Huang, K Leitzell, E. Lonnoy, J.B.R. Matthews, T. K. Maycock, T. Waterfield, O. Yelekci, R. Yu and B. Zhou (Eds.)]. Cambridge, UK: Cambridge University Press, 2021.
Jiang, Z., Li, W., Xu, J., Li, L., 2015. Extreme precipitation indices over China in CMIP5 models. Part I: model evaluation. J. Clim. 28, 8603–8619.
Jiang, Q., Li, W., Fan, Z., He, X., Sun, W., Chen, S., et al., 2021a. Evaluation of the ERA5 reanalysis precipitation dataset over Chinese Mainland. J. Hydrol. 595, 125660.
Jiang, S., Wei, L., Ren, L., Xu, C.-Y., Zhong, F., Wang, M., et al., 2021b. Utility of integrated IMERG precipitation and GLEAM potential evapotranspiration products for drought monitoring over mainland China. Atmos. Res. 247, 105141.
Jiang, J., Su, T., Liu, Y., Wu, G., Yu, W., Li, J., 2022. Southeast China extreme drought event in august 2019: context of coupling of midlatitude and tropical systems. J. Clim. 35, 7299–7313.
Koster, R., Schubert, S.D., Wang, H., Mahanama, S., Deangelis, A.M., 2019. Flash drought as captured by reanalysis data: disentangling the contributions of precipitation deficit and excess evapotranspiration. J. Hydrometeorol. 20, 1241–1258.
Lafferty, D.C., Sriver, R.L., Haqiqi, I., Hertel, T.W., Keller, K., Nicholas, R.E., 2021. Statistically bias-corrected and downscaled climate models underestimate the adverse effects of extreme heat on U.S. maize yields. Commun. Earth Environ. 2, 196.
Li, J., Wang, Z., Wu, X., Guo, S., Chen, X., 2020. Flash droughts in the Pearl River Basin, China: observed characteristics and future changes. Sci. Total Environ. 707, 136074.
Liu, Y., Zhu, Y., Zhang, L., Ren, L., Yuan, F., Yang, X., et al., 2020. Flash droughts characterization over China: from a perspective of the rapid intensification rate. Sci. Total Environ. 704, 135373.
Luo, M., Lau, N.-C., 2017. Heat waves in southern China: synoptic behavior, long-term change, and urbanization effects. J. Clim. 30, 703–720.
Mahto, S.S., Mishra, V., 2023. Increasing risk of simultaneous occurrence of flash drought in major global croplands. Environ. Res. Lett. 18, 044044.
Martens, B., Miralles, D.G., Lievens, H., van der Schalie, R., de Jeu, R.A.M., Fernández-Prieto, D., et al., 2017. GLEAM v3: satellite-based land evaporation and root-zone soil moisture. Geosci. Model Dev. 10, 1903–1925.
Martius, O., Pfahl, S., Chevalier, C., 2016. A global quantification of compound precipitation and wind extremes. Geophys. Res. Lett. 43, 7709–7717.
Meng, Y., Hao, Z., Feng, S., Zhang, X., Hao, F., 2022. Increase in compound dry-warm and wet-warm events under global warming in CMIP6 models. Glob. Planet. Chang. 210, 103773.
Miao, Y., Wang, A., 2020. A daily 0.25° × 0.25° hydrologically based land surface flux dataset for conterminous China, 1961–2017. J. Hydrol. 590, 125413.
Mishra, V., Aadhar, S., Mahto, S.S., 2021. Anthropogenic warming and intraseasonal summer monsoon variability amplify the risk of future flash droughts in India. npj Clim. Atmos. Sci. 4, 1.
Mo, K.C., 2011. Drought onset and recovery over the United States. J. Geophys. Res. Atmos. 116.
Mo, K.C., Lettenmaier, D.P., 2015. Heat wave flash droughts in decline. Geophys. Res. Lett. 42, 2823–2829.
Mohammadi, K., Jiang, Y., Wang, G., 2022. Flash drought early warning based on the trajectory of solar-induced chlorophyll fluorescence. Proc. Natl. Acad. Sci. 119, e2202767119.
Mukherjee, S., Mishra, A.K., 2022. Global flash drought analysis: uncertainties from indicators and datasets. Earth's Future 10, e2022EF002660.
Nguyen, H., Wheeler, M.C., Otkin, J.A., Frost, A.J., Stone, R.C., Cowan, T., 2019. Using evaporative stress index to monitor flash drought in Australia. Environ. Res. Lett. 6. https://doi.org/10.1088/1748-9326/ab2103.
Nguyen, H., Wheeler, M.C., Hendon, H.H., Lim, E.P., Otkin, J.A., 2021. The 2019 flash droughts in subtropical eastern Australia and their association with large-scale climate drivers. Weather. Clim. Extremes 32, 100321.
Noguera, I., Domínguez-Castro, F., Vicente-Serrano, S.M., 2020. Characteristics and trends of flash droughts in Spain, 1961–2018. Ann. N. Y. Acad. Sci. 1472, 155–172.
O, S., Park, S.K., 2023. Flash drought drives rapid vegetation stress in arid regions in Europe. Environ. Res. Lett. 18.
O'Neill, B.C., Tebaldi, C., van Vuuren, D.P., Eyring, V., Friedlingstein, P., Hurtt, G., et al., 2016. The scenario model intercomparison project (ScenarioMIP) for CMIP6. Geosci. Model Dev. 9, 3461–3482.
Osman, M., Zaitchik, B.F., Badr, H.S., Christian, J.I., Tadesse, T., Otkin, J.A., et al., 2021. Flash drought onset over the contiguous United States: sensitivity of inventories and trends to quantitative definitions. Hydrol. Earth Syst. Sci. 25, 565–581.
Otkin, J.A., Anderson, M.C., Hain, C., Mladenova, I.E., Basara, J.B., Svoboda, M., 2013. Examining rapid onset drought development using the thermal infrared-based evaporative stress index. J. Hydrometeorol. 14, 1057–1074.
Otkin, J.A., Anderson, M.C., Hain, C., Svoboda, M., Johnson, D., Mueller, R., et al., 2016. Assessing the evolution of soil moisture and vegetation conditions during the 2012 United States flash drought. Agric. For. Meteorol. 218, 230–242.
Otkin, J.A., Svoboda, M., Hunt, E.D., Ford, T.W., Anderson, M.C., Hain, C., et al., 2018. Flash droughts: a review and assessment of the challenges imposed by rapid onset droughts in the United States. Bull. Am. Meteorol. Soc. 99, 911–919.
Pereira, A.R., Pruitt, W.O., 2004. Adaptation of the Thornthwaite scheme for estimating daily reference evapotranspiration. Agric. Water Manag. 66, 251–257.
Qing, Y., Wang, S., Ancell, B.C., Yang, Z.-L., 2022. Accelerating flash droughts induced by the joint influence of soil moisture depletion and atmospheric aridity. Nat. Commun. 13, 1139.
Raghavan, S.V., Hur, J., Liong, S.-Y., 2018. Evaluations of NASA NEX-GDDP data over Southeast Asia: present and future climates. Clim. Chang. 148, 503–518.
Ridder, N., Pitman, A., Westra, S., Do, H., Bador, M., Hirsch, A., et al., 2020. Global hotspots for the occurrence of compound events. Nat. Commun. 11, 5956.
Shi, Z., Xu, X., Jia, G., 2021. Urbanization magnified nighttime heat waves in China. Geophys. Res. Lett. 48, e2021GL093603.
Sreeparvathy, V., Srinivas, V.V., 2022. Meteorological flash droughts risk projections based on CMIP6 climate change scenarios. npj Clim. Atmos. Sci. 5, 77.
Su, B., Huang, J., Fischer, T., Wang, Y., Kundzewicz, Z.W., Zhai, J., et al., 2018. Drought losses in China might double between the 1.5 °C and 2.0 °C warming. Proc. Natl. Acad. Sci. 115, 10600–10605.

Sun, P., Ma, Z., Zhang, Q., Singh, V.P., Xu, C.-Y., 2022. Modified drought severity index: model improvement and its application in drought monitoring in China. J. Hydrol. 612, 128097.
Svoboda, M., Lecomte, D., Hayes, M., Heim, R., Gleason, K., Angel, J., et al., 2002. The drought monitor. Bull. Am. Meteorol. Soc. 83, 1181–1190.
Swain, D.L., Langenbrunner, B., Neelin, J.D., Hall, A., 2018. Increasing precipitation volatility in twenty-first-century California. Nat. Clim. Chang. 8, 427–433.
Thabeet, A., Vennetier, M., Gadbin-Henry, C., Denelle, N., Roux, M., Caraglio, Y., et al., 2009. Response of Pinus sylvestris L. to recent climatic events in the French Mediterranean region. Trees 23, 843–853.
Thornthwaite, C.W., 1948. An approach toward a rational classification of climate. Geogr. Rev. 38, 55–94.
Thrasher, B., Wang, W., Michaelis, A., Melton, F., Lee, T., Nemani, R., 2022. NASA global daily downscaled projections, CMIP6. Sci. Data 9, 262.
Tian, L., Leasor, Z.T., Quiring, S.M., 2020. Developing a hybrid drought index: precipitation evapotranspiration difference condition index. Clim. Risk Manag. 29, 100238.
Trajkovic, S., Gocic, M., Pongracz, R., Bartholy, J., 2019. Adjustment of Thornthwaite equation for estimating evapotranspiration in Vojvodina. Theor. Appl. Climatol. 138, 1231–1240.
Trenberth, K.E., Dai, A., van der Schrier, G., Jones, P.D., Barichivich, J., Briffa, K.R., et al., 2014. Global warming and changes in drought. Nat. Clim. Chang. 4, 17–22.
Tripathy, K.P., Mukherjee, S., Mishra, A.K., Mann, M.E., Williams, A.P., 2023. Climate change will accelerate the high-end risk of compound drought and heatwave events. Proc. Natl. Acad. Sci. U. S. A. 120, e2219825120.
Vicente-Serrano, S.M., Beguería, S., López moreno, J.I., 2010. A multiscalar drought index sensitive to global warming: the standardized precipitation evapotranspiration index. J. Clim. 23, 1696–1718.
Wang, Y., Yuan, X., 2021. Anthropogenic speeding up of South China flash droughts as exemplified by the 2019 summer-autumn transition season. Geophys. Res. Lett. 48, e2020GL091901.
Wang, F., Lai, H., Li, Y., Feng, K., Tian, Q., Guo, W., et al., 2023a. Dynamic variations of terrestrial ecological drought and propagation analysis with meteorological drought across the mainland China. Sci. Total Environ. 896, 165314.
Wang, H., Zhu, Q., Wang, Y., Zhang, H., 2023b. Spatio-temporal characteristics and driving factors of flash drought recovery: from the perspective of soil moisture and GPP changes. Weather. Clim. Extremes 42, 100605.
Xi, X., Yuan, X., 2022. Significant water stress on gross primary productivity during flash droughts with hot conditions. Agric. For. Meteorol. 324, 109100.
Yang, X., Yong, B., Ren, L., Zhang, Y., Long, D., 2017. Multi-scale validation of GLEAM evapotranspiration products over China via ChinaFLUX ET measurements. Int. J. Remote Sens. 38, 5688–5709.
Yin, J., Gentine, P., Slater, L., Gu, L., Pokhrel, Y., Hanasaki, N., et al., 2023. Future socio-ecosystem productivity threatened by compound drought–heatwave events. Nat. Sustain. 6, 259–272.
Yu, R., Zhai, P., 2020. More frequent and widespread persistent compound drought and heat event observed in China. Sci. Rep. 10, 14576.
Yuan, X., Wang, L., Wu, P., Ji, P., Sheffield, J., Zhang, M., 2019. Anthropogenic shift towards higher risk of flash drought over China. Nat. Commun. 10, 4661.
Yuan, X., Wang, Y., Ji, P., Wu, P., Sheffield, J., Otkin, J.A., 2023. A global transition to flash droughts under climate change. Science 380, 187–191.
Zha, X., Xiong, L., Liu, C., Shu, P., Xiong, B., 2023. Identification and evaluation of soil moisture flash drought by a nonstationary framework considering climate and land cover changes. Sci. Total Environ. 856, 158953.
Zhang, Y., You, Q., Chen, C., Ge, J., 2016. Impacts of climate change on streamflows under RCP scenarios: a case study in Xin River Basin, China. Atmos. Res. 178, 521–534.
Zhang, Y., You, Q., Chen, C., Xin, L., 2017. Flash droughts in a typical humid and subtropical basin: a case study in the Gan River Basin, China. J. Hydrol. 551, 162–176.
Zhang, Y., You, Q., Mao, G., Chen, C., Ye, Z., 2019. Short-term concurrent drought and heatwave frequency with 1.5 and 2.0 C global warming in humid subtropical basins: a case study in the Gan River Basin, China. Clim. Dyn. 52, 4621–4641.
Zhang, P., Jeong, J.-H., Yoon, J.-H., Kim, H., Wang, S.Y.S., Linderholm, H.W., et al., 2020a. Abrupt shift to hotter and drier climate over inner East Asia beyond the tipping point. Science 370, 1095–1099.
Zhang, Y., Mao, G., Chen, C., Lu, Z., Luo, Z., Zhou, W., 2020b. Population exposure to concurrent daytime and nighttime heatwaves in Huai River Basin, China. Sustain. Cities Soc. 61, 102309.
Zhang, Y., You, Q., Mao, G., Chen, C., Li, X., Yu, J., 2021. Flash drought characteristics by different severities in humid subtropical basins: a case study in the Gan River Basin, China. J. Clim. 34, 7337–7357.
Zhang, S., Li, M., Ma, Z., Jian, D., Lv, M., Yang, Q., et al., 2023a. The intensification of flash droughts across China from 1981 to 2021. Clim. Dyn. https://doi.org/10.1007/s00382-023-06980-8.
Zhang, Y., You, Q., Ullah, S., Chen, C., Shen, L., Liu, Z., 2023b. Substantial increase in abrupt shifts between drought and flood events in China based on observations and model simulations. Sci. Total Environ. 876, 162822.
Zhou, S., Williams, A.P., Berg, A., Cook, B.I., Zhang, Y., Hagemann, S., et al., 2019. Land-atmosphere feedbacks exacerbate concurrent soil drought and atmospheric aridity. Proc. Natl. Acad. Sci. U. S. A. 116, 18848–18853.
Zhu, H., Jiang, Z., Li, L., 2021. Projection of climate extremes in China, an incremental exercise from CMIP5 to CMIP6. Sci. Bull. 66, 2528–2537.
Zscheischler, J., Martius, O., Westra, S., Bevacqua, E., Raymond, C., Horton, R.M., et al., 2020. A typology of compound weather and climate events. Nat. Rev. Earth Environ. 1, 333–347.